FLOW PAST SPHERE TRAINS

AN EXPERIMENTAL STUDY
OF INCOMPRESSIBLE TURBULENT FLOW
IN PIPES CONTAINING SPHERE TRAINS

BY

E. N. TAWO, B.Sc.(Eng.) Wales

A Thesis

Submitted to the Faculty of Graduate Studies

in Partial Fulfilment of the Requirements

for the Degree

Master of Engineering

McMaster University

(November) 1969

MASTER OF ENGINEERING (1969) McMASTER UNIVERSITY

(Mechanical Engineering) Hamilton, Ontario.

TITLE: AN EXPERIMENTAL STUDY OF INCOMPRESSIBLE TURBULENT FLOW IN PIPES CONTAINING SPHERE TRAINS.

AUTHOR: Edom Neji TAWO, B.Sc.(Eng.)

SUPERVISOR: Dr. G.F. ROUND

NUMBER OF PAGES: ix + 88

SCOPE AND CONTENTS: The pressure gradients for sphere trains in 1 in. and 2 in. pipes have been measured with water flowing past the stationary spheres at Reynolds numbers (based on pipe diameter) from 10^4 - 10^5, and sphere/pipe diameter ratios ranging from 0.486 - 0.84. Two dimensionless pressure ratios have been derived so that the experimental results obtained can be generalised to any pipe diameter with the above constraints on Reynolds number and diameter ratio. Drag coefficients have also been calculated from pressure drop measurements for the 0.84 diam. ratio spheres in 1 in. pipe. These have been compared with McNoun's drag coefficient.

The application of the results to predict pressure gradients for sphere trains in any pipe diameter has been illustrated.

ACKNOWLEDGEMENTS

The Author gratefully acknowledges the guidance and encouragement given by Dr. G.F. Round.

Thanks also to Miss L. Fagan for the assistance especially in typing this thesis.

The Research for this thesis was supported in part by both the Defence Research Board of Canada, Grant No. 9550 - 42 and the National Research Council of Canada under Grant No. A5183.

TABLE OF CONTENTS

TABLE OF CONTENTS (cont'd)

LIST OF FIGURES

LIST OF TABLES

NOMENCLATURE

PR1, PR2	Pressure ratios based on free pipe pressure gradient and annulus pressure gradient respectively
f	Friction factor
ρ	Density
g	Acceleration due to gravity = 32.2 ft./sec.^{2}
V_o	Mean flow velocity in the free pipe
D, d	Pipe diameter and sphere diameter respectively in inches
R_e, R_{e_N}	Reynolds number based on pipe diameter
$\frac{dp}{dz}$	Pressure gradient in the axial direction of flow
ν	Kinematic viscosity in ft.^{2}/sec.
$\left(\frac{dp}{dz}\right)_{LIQ.}$	Pressure gradient with no spheres present in the pipe
ΔP_s	Pressure drop with spheres located in the pipe
L	Distance between points from which pressure drop is measured
$P_{\varepsilon 1}$, $P_{\varepsilon 2}$	Pressure drops due to the end effects
'N-sphere system'	Theoretically it refers to an infinitely long sphere train. In practice it is the arrangement whereby pressure drops are measured within the length of the annulus
$\left(\frac{dp}{dz}\right)_{corr.}$, DPZC	Pressure gradient based on the length of the sphere train

NOMENCLATURE (cont'd)

IGPM	Imperial gallons per minute
DPZCL	Pressure gradient based on L with spheres located in the pipe; in inches water per inch.
n	No. of spheres making up the train
C_D^*	Drag coefficient in the bounded medium
$\left(\frac{dp}{dz}\right)_n$, $\left(P_{1n}-P_{2n}\right)/L$, DPZN	N-sphere pressure gradient in ins./in.

ABSTRACT

A series of experiments was made to measure the pressure drop across stationary sphere trains located in 1 in. and 2 in. smooth pipes through which water was flowing. The size of spheres used ranged from ½ in. to 1½ in. in diameter; sphere-pipe diameter ratios were 0.486, 0.60, 0.737 and 0.84, while the effective Reynolds number based on pipe diameter ranged from 10^4 to 10^5. The length of sphere train, for each diameter ratio, was adjusted by varying the number of spheres from 1 through to 12.

Two dimensionless pressure ratios, PR1 and PR2, were derived to relate the pressure gradient with spheres located in the pipe to the pressure gradient with spheres absent. These enable the experimental results to be of general application to any pipe diameter, with Reynolds numbers in the above range and sphere-pipe diameter ratios ranging from 0.486 - 0.84. PR1 pertains theoretically to the pressure gradient for an infinitely long sphere train. It was approximated in practice by measuring the pressure gradient within the length of the sphere trains, i.e. by locating pressure taps such that they were unaffected by end effects, and was found to be a function of diameter ratio-varying linearly on a log-scale when plotted against the Reynolds number.

PR2 is a function of the number of spheres making up a train, the diameter ratio, and the Reynolds number. It was observed that PR2 decreased with increase in the number of spheres. It also tended to decrease with increase in diameter ratio for a given number of spheres at a given Reynolds number. Pressure gradients based on the length of sphere train were plotted together with the end effect parameters. Drag coefficients were calculated from pressure drop measurements for the 0.84 diameter ratio, and compared with McNoun's theoretical equation. The discrepancy was less than 10% for Reynolds numbers greater than 8×10^4. Less good agreement was observed at lower Reynolds numbers and diameter ratios. Finally it is shown how the PR1 and PR2 relations may be used to predict the flow conditions in any smooth pipe with spheres located in them, for the Reynolds number range 10^4 - 10^5 and sphere-pipe diameter ratios 0.486 - 0.84.

1. INTRODUCTION

A substantial amount of literature exists on the viscous flow past spheres, particularly at low Reynolds numbers (1-12), but to date no research work has been reported on the flow past trains of spheres at Reynolds numbers > 100. Most of the previous work has concentrated on multi-particle assemblies relating to sedimentation, fluidization and other so-called 'creeping motion' phenomena. The transportation of capsules in pipelines has however roused interest on the turbulent flow past spheres in pipes. The Research Council of Alberta has been largely responsible for work that has been done in this area so far, and the papers published by the researchers at the Research Council have dealt extensively with the flow of cylindrical capsules and single spheres. In a series of papers having the general title "The Pipeline Flow of Capsules" (16-26), the emphasis has been on the determination of the capsule velocity or velocity ratio (capsule/free stream) as a function of average velocity, diameter ratio, and capsule/liquid density ratio. Some of the concepts in

---

* The word 'capsule' in this context has come to mean a large, regularly shaped body - hollow or solid, cylindrical or spherical in shape - whose minor diameter is comparable to the diameter of the pipe in which it is travelling.

the present study like 'pressure ratio' (see Chapter 2), have been influenced by the terminology contained in these papers.

In designing a pipeline to transport solid materials or capsules, one would in the first instance be interested in predicting the pressure gradient and subsequently the power consumption. The following study relates to this in that it essentially consists of determining experimentally the pressure gradients associated with stationary fully eccentric spheres in a turbulent flow field, as the number of spheres making up the train increases and the sphere/pipe diameter ratio varies. A correlation has been developed so that the data collected could be related to behaviour for pipe diameters other than those used in the present study. Some considerations of drag coefficients have also been made.

2. THEORY

2.1. Pressure Gradient in a Free Pipe

The DARCY-WEISBACH equation may be written in the form,

$$\frac{dp}{dz} = \frac{f}{D} \cdot \rho \frac{Vo^2}{2g} \qquad (2.1.1)$$

The above equation applies to any steady incompressible flow whether laminar or turbulent.

The BLASIUS equation for friction factor in turbulent flow is given as

$$f = \frac{0.316}{R_e^{1/4}} \qquad (2.1.2)$$

This equation approximates the friction factor - Reynolds number plot (Moody diagram) over the region in which we are interested. We may therefore expect a slight variation on the Reynolds number exponent in experimental work.

Substituting (2.1.2) in (2.1.1)

$$\left(\frac{dp}{dz}\right)_{LIQ} = \frac{0.316}{R_e^{1/4}} \cdot \frac{Vo^2}{2gD}$$

But $Vo = \frac{R_e \nu}{D}$

$$\left(\frac{dp}{dz}\right)_{LIQ} = \frac{0.316 \rho R_e{}^2 \nu^2}{R_e^{1/4} \; 2gD^3}$$

Now, if ν is in $ft^2/sec.$

$$\left(\frac{dp}{dz}\right)_{LIQ} = \frac{0.316 \times 144^2}{2 \times 386} \times \frac{R_{eN}^{1.75} \nu^2}{D^3} = \frac{0.316 \rho R_e^{1.75} \nu^2}{2gD^3}$$

If we substitute

$$R_e' = 10^{-4} \times R_e$$

$$\text{and } \nu' = 10^5 \times \nu$$

$$\left(\frac{dp}{dz}\right)_{LIQ} = K_1 \left(\frac{\nu'^{2} R_e'^{1.75}}{D^3}\right) \qquad (2.1.3)$$

where $K_1 = \left(\frac{0.316 . \rho}{2g}\right)$

The exponent of R_e in equation (2.1.3) in practice is not constant at 1.75 but varies between 1.7 and 2.0 (27)

2.2 Pressure Gradient with Spheres Present

For stationary spheres located in a pipe with fluid flowing past them, we would expect the pressure drop measured to be a function of

(a) The sphere diameter and number, d and n

(b) The viscosity and density of the flowing fluid μ and ρ

(c) The velocity of the fluid, Vo

(d) The spacing between the spheres

(e) The pipe diameter, D, and the relative displacements of the spheres from the centre line of the pipe; in other words, the eccentricity

(f) The location of the pressure taps

Where condition (d) is kept constant, a dimensional analysis indicates that $\Delta P_s = f\left(n, \frac{d}{D}, R_e, L\right)$ (2.2.1)

To define equation (2.2.1) we shall look more closely at the possible sphere arrangements. (cf. Fig. 1)

Case A - Single sphere

We shall define the term 'end effect zone' as the zone upstream and downstream of a sphere train within which there is significant deviation from the relationship given by equation (2.1.3). Theoretically, the downstream zone could exist for a very large number of pipe diameters. In the case of one sphere, the end effect zone is of length ℓ_2 as shown in Fig. 1.

The pressure drop between BC,

$$\Delta P_{B-C} = \left(P_{11}-P_{21}\right) - \left(\frac{dp}{dz}\right)_{LIQ}\left(\ell_1 + \ell_3\right) \qquad (2.2.4)$$

$$\left(\frac{dp}{dz}\right)_{s1} = \frac{\Delta P_{B-C}}{\ell_2} = \left(\frac{P_{11}-P_{21}}{\ell_2}\right) - \left(\frac{dp}{dz}\right)_{LIQ}\left(\frac{\ell_1+\ell_3}{\ell_2}\right) \qquad (2.2.A1)$$

Also $\ell_1 + \ell_2 + \ell_3 = L$

Case B - two spheres

Pressure drop across BC,

$$\Delta P_{B-C} = \left(P_{12}-P_{22}\right) - \left(\frac{dp}{dz}\right)_{LIQ}\left(\ell_{12}+\ell_{32}\right) \qquad (2.2.B)$$

$$\left(\frac{dp}{dz}\right)_{s2} = \frac{\Delta P_{B-C}}{\ell 22} = \left(\frac{P_{12}-P_{22}}{\ell 22}\right) - \left(\frac{dp}{dz}\right)_{LIQ}\left(\frac{\ell_{12}+\ell_{32}}{\ell 22}\right) \qquad (2.2.B1)$$

Case C - three or more spheres

Here is a situation in which the pressure taps may conceivably lie within the end effect zones. The pressure drop measured cannot be predicted semi-empirically as we have done in (A) and (B). However, we would expect a sudden drop in the value of P_1, and $P_{\varepsilon 1}$ and $P_{\varepsilon 2}$ should be about the same for 3, 4, 5, ...20 or more spheres.

Case D - n - spheres

In this case, as far as end effects on the pressure taps is concerned $n \rightarrow \infty$ i.e. the end effects are remote from P_{1n} and P_{2n}. The pressure gradient for an 'n-sphere' system is

$$\left(\frac{dp}{dz}\right)_n = \left(\frac{P_{1n}-P_{2n}}{L}\right) \qquad (2.2.D)$$

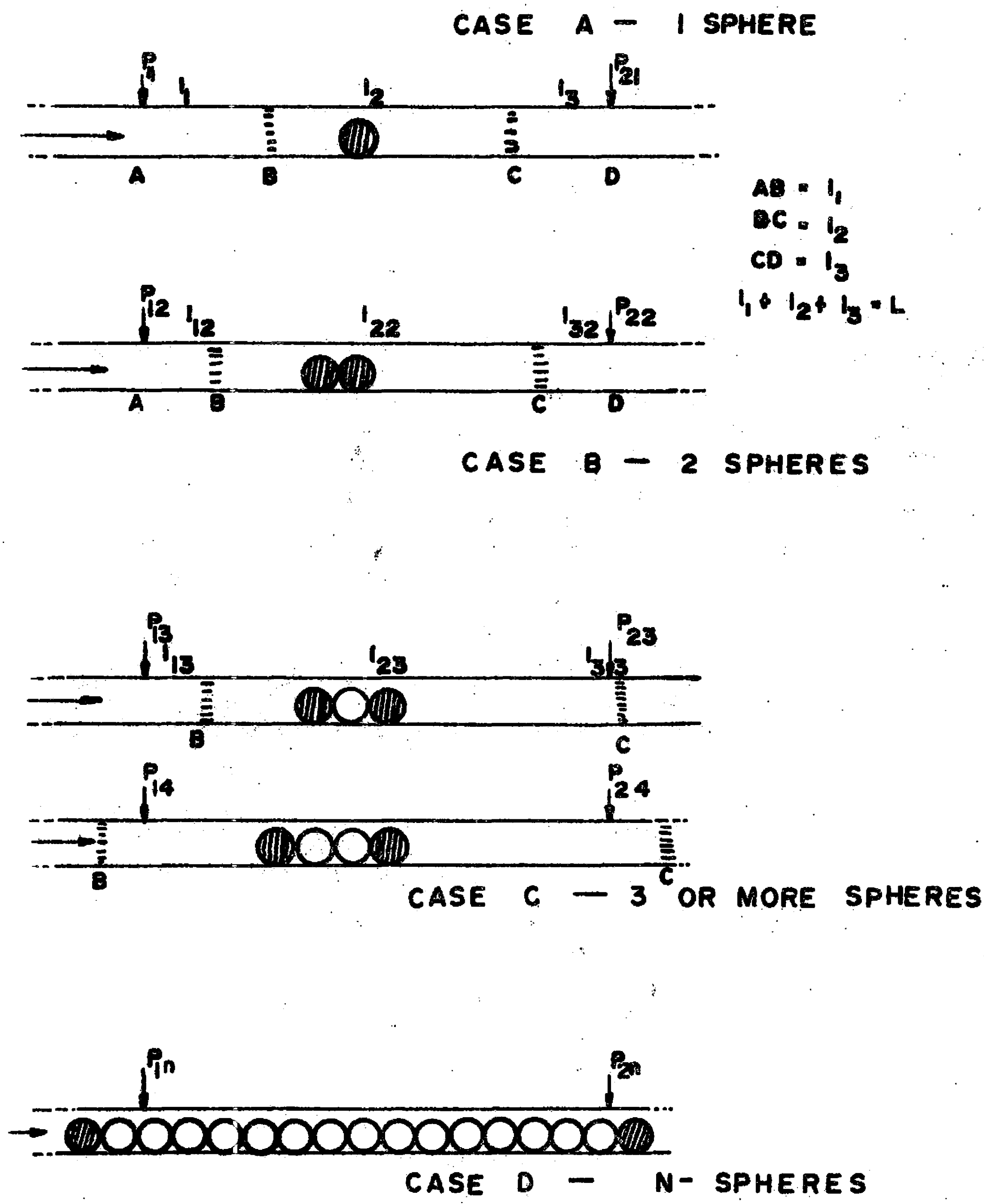

FIGURE NO·1

ARRANGEMENT OF SPHERES

Having considered case A, B, C and D, it is clear that we have two general arrangements in which the pressure gradient can be handled semi-empirically: The arrangement in which pressure taps lie beyond the end effect zones; and the 'n-sphere system'. The latter pressure gradient is represented by equation (2.2.D); but in order to generalize the former for any number of spheres, we make the following assumption:- Let end effect pressure drops for any number of spheres in the train of given diameter be constant for a given Vo and given by $P_{\varepsilon 1}$ and $P_{\varepsilon 2}$.

Then the pressure drop for case B can be expressed as

$$\Delta P_{B-C2} = \left(\frac{P_{1n}-P_{2n}}{L}\right) \times d + \left(P_{\varepsilon 1}+P_{\varepsilon 2}\right) + \left(\frac{dp}{dz}\right)_{LIQ} \left(\ell_{12}+\ell_{32}\right)$$

Similarly if P_{13} and P_{23} are placed beyond the end effect zones,

$$\Delta P_{B-C_3} = \left(\frac{P_{1n}+P_{2n}}{L}\right) \times 2d + \left(P_{\varepsilon 1}+P_{\varepsilon 2}\right) + \left(\frac{dp}{dz}\right)_{LIQ} \left(\ell_{13}+\ell_{33}\right)$$

Also $$\Delta P_{B-C_4} = \left(\frac{P_{1n}+P_{2n}}{L}\right) \times 3d + \left(P_{\varepsilon 1}+P_{\varepsilon 2}\right) + \left(\frac{dp}{dz}\right)_{LIQ} \left(\ell_{14}+\ell_{34}\right)$$

In general, the pressure drop measured when pressure taps are placed beyond end-effect zones of a given sphere train is

$$\Delta P_n = \left(\frac{P_{1n}-P_{2n}}{L}\right) \cdot (n-1)d + \left(P_{\varepsilon 1}+P_{\varepsilon 2}\right) + \left(\frac{dp}{dz}\right)_{LIQ} \left(\ell_{1n}+\ell_{3n}\right) \tag{2.2.2}$$

Case A, i.e. $n = 1$, is a special case of equation (2.2.2); for then

$$\left[\Delta P_1 - \left(\frac{dp}{dz}\right)_{LIQ} \times \left(\ell_{11}+\ell_{31}\right)\right] = \left(P_{\varepsilon 1}+P_{\varepsilon 2}\right) \tag{2.2.3}$$

If we could determine the unknowns ℓ_{1n}, ℓ_{3n}, $P_{\varepsilon 2}$, we would be able to predict the pressure drop across any sphere train in which the pressure taps are placed beyond the end-effect zones, knowing the 'N-sphere' pressure gradient. To do so, another assumption will be made which is necessary to verify experimentally: that $(\varepsilon_1+\varepsilon_2)$ is constant for any number of spheres of given diameter making up the sphere train at a given velocity. In general,

$$(\ell_{1n}+\ell_{3n}) + (\varepsilon_1+\varepsilon_2) + (n-1)d = L \tag{2.2.4}$$

Some work has been done on the wake behind a sphere at low Reynolds numbers (TANEDA (6)). At a sphere Reynolds number of 100, Taneda found $(\varepsilon_{2/d})$ approximately proportional to the logarithm of the Reynolds number. But whether or not these results apply to pipe flow (with boundary effect), and whether they can be extrapolated to the high Reynolds numbers (10^4 - 10^5) in the present study is still to be verified experimentally. A possible experimental technique would be to move the pressure taps in small steps away from both ends of the sphere train and note the distances ℓ_1 and ℓ_3, at which there is significant change in pressure gradient.

2.3 End Effects

Equation (2.2.2) can be re-written in the form

$$\Delta P_n - \left(\frac{dp}{dz}\right)_{LIQ} \times \left(\ell_{1n}+\ell_{3n}\right) = \left(\frac{P_{1n}-P_{2n}}{L}\right)\left(n-1\right)_d + \left(P_{\varepsilon 1}+P_{\varepsilon 2}\right)$$

Since $\Delta P_n \gg \left(\frac{dp}{dz}\right)_{LIQ}\left(L-nd\right)$, we can replace $\left(\ell_{1n}+\ell_{3n}\right)$ by (L-nd).

Then $$\Delta P_n - \left(\frac{dp}{dz}\right)_{LIQ} (L-nd) = \left(\frac{P_{1n}-P_{2n}}{L}\right)\left(n-1\right)_d + \left(P_{\varepsilon 1}+P_{\varepsilon 2}\right)$$

(2.3.1)

The term, $\left(\frac{dp}{dz}\right)_{LIQ}\left(L-n.d\right)$, becomes increasingly insignificant relative to the total pressure drop as the length of train increases.

Dividing both sides of (2.3.1) by n.d, we obtain

$$\left(\frac{\Delta P_n}{n.d}\right) - \left(\frac{dp}{dz}\right)_{LIQ} \times \left(\frac{L-nd}{nd}\right) = \left(\frac{P_{1n}-P_{2n}}{L}\right)\left(1-\frac{1}{n}\right) + \left(\frac{P_{\varepsilon 1}+P_{\varepsilon 2}}{nd}\right) = \left(\frac{dp}{dz}\right)_{corr.}$$

(2.3.2)

What equation (2.3.2) expresses is the pressure gradient due to the sphere train's presence, i.e. apart from pipe wall friction over the length (L-nd). The pressure gradient obtained thus is independent of how far the pressure taps are away from the ends of the train, provided of course, that they lie outside the end effect zones.

$(P_{\varepsilon 1}+P_{\varepsilon 2})$ can be further reduced analytically by considering the Bernoulli effects at the nose and tail of the sphere train: Referring to Fig. 2b, we can approximate $P_{\varepsilon 1}$ as due only to the Bernoulli effect; i.e.

$$P_{\varepsilon 1} = \rho\left(\frac{V_1^{\,2}-V_o^{\,2}}{2g}\right) \qquad (2.3.4)$$

For the tail end effect, however, there are other head losses which must be taken into account in the Bernoulli equation: so that

$$\frac{P_{\varepsilon 2}}{\rho} = h_L + \left(\frac{V_o^{\,2}-V_1^{\,2}}{2g}\right) \qquad (2.3.5)$$

Adding equations (2.3.4) and (2.3.5), we still find that there is a head loss term which can only be determined experimentally.

We shall therefore adopt the approach of rearranging equation (2.3.2) to the form

$$\left(\frac{P_{\varepsilon 1}+P_{\varepsilon 2}}{nd}\right) = \left(\frac{\Delta P_n}{n.d}\right) - \left(\frac{dp}{dz}\right)_{LIQ}\left(\frac{L-n.d}{n.d}\right) - \left(\frac{P_{1n}-P_{2n}}{L}\right)\left(1-\frac{1}{n}\right) \tag{2.3.6}$$

so that the end effects can be evaluated from experimental data.

2.4 The Concept of Pressure Ratios, PR1 and PR2

Just as the free pipe pressure gradient is a function of R_e, ν, and D, (see equation (2.1.3)) so we would expect the 'N-sphere' pressure gradient to be a function of the variables R_e, ν, and an equivalent diameter d_e. The equivalent diameter is a function of sphere diameter d and pipe diameter D. The reasoning behind the first statement above, is that we can think of the flow in the 'N-sphere' system as that through a pipe of undular cross-section, with the sphere surfaces as part of the pipe inner wall. If our aim is to obtain general results which apply to all pipe diameters, and are not dependent on temperature (as ν is) then we will have to introduce other non-dimensional parameters

$$\text{Let PRESSURE RATIO, PR1} = \frac{\text{'N-SPHERE' PRESSURE GRADIENT}}{\text{FREE PIPE PRESSURE GRADIENT}}$$

$$\text{i.e. PR1} = \frac{\left(P_{1n}-P_{2n}\right)/L}{\left(DP/DZ\right)_{LIQ}} \tag{2.4.1}$$

where the numerator and denominator correspond to the same Reynolds number. To show that PR1 is truly independent of D, ν and R_e, but a function of diameter ratio, $\frac{d}{D}$, only; we shall ultimately resort to experiment. Meanwhile, on the basis of the equivalent diameter concept we shall carry out a simple analysis to derive an expression for $(P_{1n}-P_{2n})/L$ in the same way that the free pipe pressure gradient (see equation 2.1.3) was obtained. Such an analysis of turbulent flow in an eccentric, three-dimensional annulus does not appear to have been made. In any case, the following derivation gives us some insight into the nature of the 'n-sphere' pressure gradient and the pressure ratio, PR1:- Consider the fluid element IJKL (in three dimensions) shown in Fig. 2a.

Mean cross-sectional area, $A = \dfrac{\text{Vol. of Element}}{\text{Length}}$

$$= \frac{1}{d}\left[\frac{\pi D^2}{4} \cdot d - \frac{4}{3}\pi\left(\frac{d}{2}\right)^3\right]$$

$$A = \pi\left[\frac{D^2}{4} - \frac{d^2}{6}\right]$$

Surface area, $S = \pi D.d + 4\pi\left(\frac{d}{2}\right)^2$

$$= \pi d\left(D+d\right)$$

Assume that there are no other effects on the fluid element than those due to normal pressure drop and wall shear stress. Resolving forces in the direction of flow,

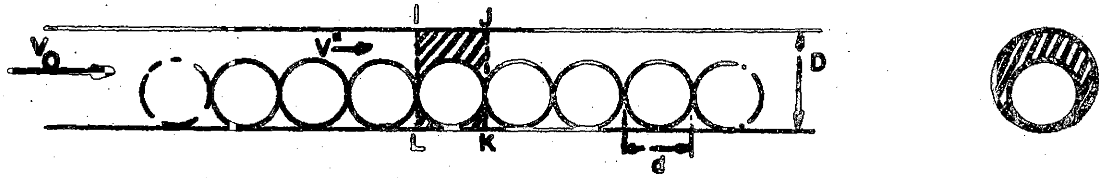

FIGURE 2a

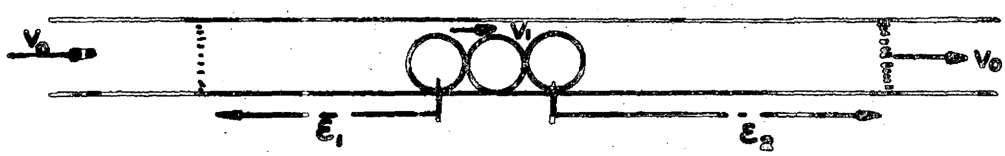

FIGURE 2b

DEFINITION DIAGRAMS

$$A(-\Delta P) = \tau_\omega \cdot S$$

where τ_ω is shear stress, and steady flow prevails.

By definition, $4\tau_\omega = f'' \cdot \rho \frac{V''^2}{2g}$ where double prime refers to values in the annulus.

$$\Delta P = \frac{f''}{4} \cdot \rho \frac{V''^2}{2g} \cdot \frac{S}{A}$$

Comparing this equation with the Darcy-Weisbach equation, the equivalent diameter, $d_e = \frac{4A}{S} \cdot d$ since d is the length of the fluid element.

$$\therefore \; d_e = \frac{\pi \left[D^2 - \frac{2}{3}d^2\right]}{d(D+d)} \cdot d$$

$$d_e = (D^2 - \tfrac{2}{3}d^2)/(D+d) \qquad (2.4.2)$$

Now, $V'' = \frac{R_e \cdot \nu}{d_e}$ and by continuity,

$$V'' \times \pi \left(\frac{D^2}{4} - \frac{d^2}{6}\right) = Vo \times \frac{\pi D^2}{4} = \pi \cdot \frac{R_e . D . \nu}{4}$$

since $R_e = \frac{V_o \, D}{\nu}$

$$\therefore \; V'' = R_e \cdot \frac{D\nu}{\left(D^2 - \frac{2}{3}d^2\right)} = \frac{D^2}{\left(D^2 - \frac{2}{3}d^2\right)} \cdot Vo \qquad (2.4.3)$$

and since $V'' = \frac{R''_e \cdot \nu}{d_e}$ by substituting for V" and d_e in equation (2.4.3),

$$R''_e = \left(\frac{D}{D+d}\right) \cdot R_e \qquad (2.4.4)$$

We have obtained above the relation,

$$\Delta P = \frac{f''}{4} \cdot \rho \frac{V''^2}{2g} \cdot \frac{S}{A} \text{ where } S = \pi D(d+D) \text{ and } A = \pi\left(\frac{D^2}{4} - \frac{d^2}{6}\right).$$

'N-sphere' pressure gradient,

$$\left(\frac{P_{1n}-P_{2n}}{L}\right) = \frac{\Delta P}{d} = \frac{f''}{4} \cdot \rho \frac{V''^2}{2g} \cdot \frac{D}{d}\left(\frac{d+D}{\frac{D^2}{4}-\frac{d^2}{6}}\right) \qquad (2.4.5)$$

If $4 \times 10^3 < R''_e < 10^5$, as we expect it will be for R_e between 10^4 and 10^5 (See equation 2.4.4) then BLASIUS equation for friction factor can be used to replace f'':

$$f'' = \frac{0.316}{R_e''^{\frac{1}{4}}} = \frac{0.316}{\left(\frac{D}{D+d} \cdot R_e\right)^{\frac{1}{4}}} \qquad (2.4.6)$$

Substituting (2.4.6) and (2.4.3) in (2.4.5) we obtain

$$\left(\frac{P_{1n}-P_{2n}}{L}\right) = \left(\frac{0.316 \times 144^2 \nu^2}{2g}\right) \cdot \frac{(D+d)^{1.25}}{\left(D^2 - \frac{2}{3}d^2\right)^3} \cdot \left(D \times R_e\right)^{1.75}$$

$$= k_1' \nu^2 \frac{\left(1 + \frac{d}{D}\right)^{1.25} \times D^3}{\left[1 - \frac{2}{3}\left(\frac{d}{D}\right)^2\right]^3 \times D^6} \cdot R_e^{1.75}$$

$$= k_1^{\prime} \frac{\left(1 + \frac{d}{D}\right)^{1.25}}{\left[1 - \frac{2}{3}\left(\frac{d}{D}\right)^2\right]^3} \cdot \frac{\nu R_e^{1.75}}{D^3}$$

As in equation (2.1.3), if we substitute

$$R_e' = 10^{-4} \times R_e$$

$$\text{and} \quad \nu' = 10^5 \times \nu$$

$$\left(\frac{P_{1n}+P_{2n}}{L}\right) = k_1 \left\{\frac{\left(1 + \frac{d}{D}\right)^{1.25}}{\left[1 - \frac{2}{3}\left(\frac{d}{D}\right)^2\right]^3}\right\}\left(\frac{\nu'^2 R_e'^{1.75}}{D^3}\right) \qquad (2.4.7)$$

where $k_1 = 8.487 \times 10^3$

Divide equation (2.4.7) by (2.1.3) we find that

$$PR1 = \left(1 + \frac{d}{D}\right)^{1.25} \Big/ \left\{1 - \left(\frac{2}{3}\right)\left(\frac{d}{D}\right)^2\right\}^3 \qquad (2.4.8)$$

That is, PR1 is a function of dia. ratio only. Equation (2.4.8) satisfies the boundary condition that when diameter ratio, $\frac{d}{D}$, equals zero PR1 equals 1; meaning that we then have a free pipe pressure gradient.

A second pressure ratio (PR2) is defined for the set-up whereby the pressure taps lie beyond the end-effect zones:-

$$PR2 = ((DP/DZ)corr.)/((P_{1n}-P_{2n})/L) \qquad (2.4.9)$$

The numerator is given in equation (2.3.2) as

$$\left(\frac{dp}{dz}\right)_{corr.} = \left(\frac{P_{1n}-P_{2n}}{L}\right) \cdot \left(1 - \frac{1}{n}\right) + \left(\frac{P_{\varepsilon 1}+P_{\varepsilon 2}}{nd}\right)$$

$$\text{So } PR2 = 1 - \frac{1}{n} + \left(\frac{P_{\varepsilon 1}+P_{\varepsilon 2}}{P_{1n}+P_{2n}}\right) \cdot \frac{L}{nd}$$

$$PR2 = 1 + \frac{1}{n}\left\{\left(\frac{\left(P_{\varepsilon 1}+P_{\varepsilon 2}\right)/d}{\left(P_{1n}-P_{2n}\right)/L}\right) - 1\right\} \tag{2.4.10}$$

Equation (2.4.10) cannot be reduced analytically any further since $P_{\varepsilon 1}+P_{\varepsilon 2}$ can be obtained only empirically.

2.5 Considerations of Drag of the Sphere Train

The total drag on the fluid as it flows past the sphere train comprises the skin friction on the surface of the spheres, pipe wall friction, and drag due to distortion of the flow.

In order to evaluate the drag coefficient of the sphere or sphere train in a pipe, we need to separate total pipe wall friction drag from the drag measurable through pressure drops. This is not a simple matter, as the following discussion wil show. The pressure drop $\Delta P_s = (P_1-P_2)$ over a length, L, of tube may be thought of as being composed of three components: (cf. Fig. 3a)

(i) The pressure drop ΔP_L due to the liquid flowing in the tube without the sphere present. This is easily calculated from the Darcy-Weisbach formula.

(ii) The pressure drop ΔP_m associated with distortion of the flow and energy dissipation in the wake.

(iii) A pressure drop ΔP_L^1 which is caused by a change in the shear stress distribution on the pipe wall in the vicinity of the sphere due to the change of flow velocity. A liquid flowing in a tube without a sphere experiences uniform wall stress from cross-section to cross-section.

Figure 3a illustrates the point that to obtain ΔP_m, and hence the drag coefficient, ΔP_L and $\Delta P_L{}^1$ will have to be subtracted from (P_1-P_2). Since there is no feasible way of evaluating $\Delta P_L{}^1$, the only practical way to obtain drag coefficients will be to measure the drag force directly using force transducer; or suspend the spheres in inclined tubes as Round and Kruyer (28) have done. Nevertheless, on the basis of the following analysis, an estimate of the drag coefficient for single spheres in the pipes can be made:-

The drag force, by definition, is given as

$$F_D = C_D^* \cdot \left(\frac{\pi d^2}{4}\right) \cdot \frac{\rho Vo^2}{2g} \qquad (2.5.1)$$

The asterisk on C_D is used to distinguish it from the drag coefficient of a sphere in an unbounded medium.

The converging flow upstream from the sphere's equator is essentially irrotational; so we can apply the Bernoulli equation (See Fig. 3b).

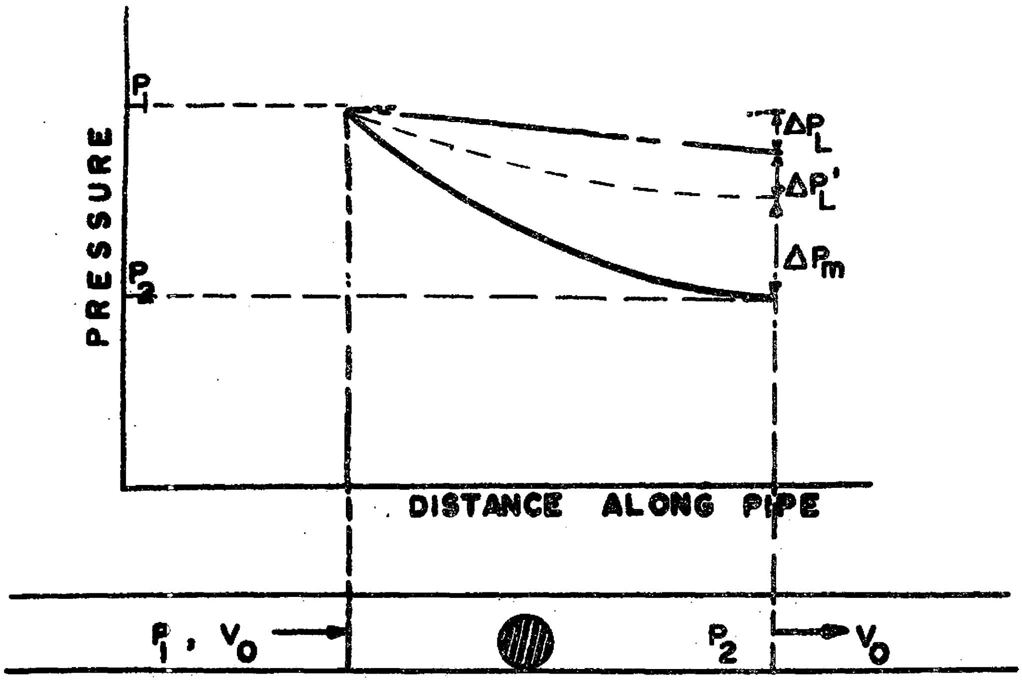

FIGURE 3a

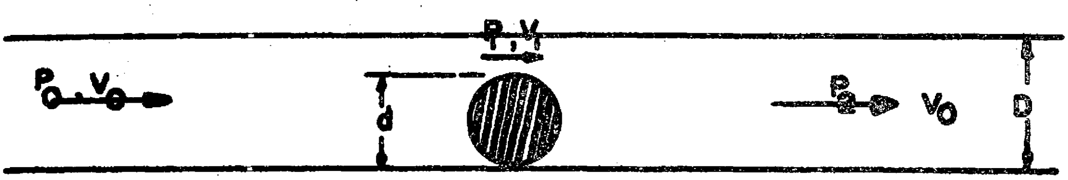

FIGURE 3b

DEFINITION DIAGRAMS

$$p_o + \rho\frac{V_o^2}{2} = p_1 + \rho\frac{V_1^2}{2} \qquad (2.5.1a)$$

by continuity,

$$V_o \cdot \frac{\pi D^2}{4} = V_1 \cdot \frac{\pi}{4}(D^2-d^2)$$

$$\text{i.e.} \quad V_o . D^2 = V_1(D^2-d^2) \qquad (2.5.2)$$

If the pressure over the downstream face of the sphere is assumed to be equal to p, as in the analysis of an abrupt pipe expansion, the momentum equation can be applied between points 1 and 2 (Fig. 3b).

$$(p_2-p_1)\pi D^2/4 = \rho Q(V_1-V_o) \qquad (2.5.3)$$

The momentum equation can again be applied for points 0 and 2, whereby a relationship between the total pressure drop and the drag force is obtained:

$$(p_o-p_2)\pi D^2/4 = F_D \qquad (2.5.4)$$

Relating (2.5.1) and (2.5.4),

$$C_D = \frac{D^2}{d^2}\left(\frac{p_o-p_2}{V_o^2/2g}\right) \qquad (2.5.5)$$

Substitute (2.5.2) in (2.5.1a) and (2.5.3):

$$(p_o-p_1)/\rho = \tfrac{1}{2}V_1^2\left[1-\left(\frac{D^2-d^2}{D^2}\right)^2\right]$$

$$(p_2-p_1)/\rho = \left(\frac{D^2-d^2}{D^2}\right) \cdot V_1^2\left[1-\left(\frac{D^2-d^2}{D^2}\right)\right]$$

$$\therefore \quad \frac{(P_o - P_2)}{\rho} = V_1^{\,2}\left\{ \tfrac{1}{2}\left[1-\left(\frac{D^2-d^2}{D^2}\right)^2\right] - \left(\frac{D^2-d^2}{D^2}\right) + \left[\frac{D^2-d^2}{D^2}\right]^2 \right\}$$

$$= \left(\frac{D^2}{D^2-d^2}\right)^2 V_o^{\,2}\left\{ \tfrac{1}{2}\left[1+\left(\frac{D^2-d^2}{D^2}\right)^2\right] - \left(\frac{D^2-d^2}{D^2}\right) \right\}$$

$$= \left(\frac{D^2}{D^2-d^2}\right)^2 \frac{Vo^2}{2g}\left[1-\left(\frac{D^2-d^2}{D^2}\right)\right]^2 = \left(\frac{D^2}{D^2-d^2}\right)^2 \cdot \frac{Vo^2}{2g} \cdot \left(\frac{d}{D}\right)^4$$

Now substitute this and (2.5.1) in equation (2.5.4):

$$C_D^* \cdot \frac{\pi d^2}{4} \cdot \rho\frac{Vo^2}{2g} = \rho\frac{Vo^2}{2g} \cdot \left(\frac{d}{D}\right)^4\left(\frac{D^2}{D^2-d^2}\right)^2 \cdot \frac{\pi D^2}{4}$$

$$\therefore \quad C_D^* = \left[\frac{\frac{d}{D}}{1-\left(\frac{d}{D}\right)^2}\right]^2 \tag{2.5.6}$$

$$(p_o - p_2) = \rho\frac{Vo^2}{2g} \cdot \left[\frac{\left(\frac{d}{D}\right)^2}{1-\left(\frac{d}{D}\right)^2}\right]^2 \tag{2.5.7}$$

It is evident that the assumptions made in the derivation of (2.5.5) and (2.5.6) are justifiable only if $\frac{d}{D}$ is near unity. Observations by McNoun and Newlin (15) show that equations (2.5.5) and (2.5.6) agree well with experiment for diameter ratios greater than 0.8.

Correlations by Round and Kruyer (28) will also be useful in checking pressure drops within the approximate diameter ratio range as will equation (2.5.7).

3. APPARATUS AND EXPERIMENTAL PROCEDURE

3.1. General Requirements

The hydraulic system illustrated in Fig. 4 was designed to meet the following requirements:-

(i) The water flow velocity could be varied between 0 and 12 ft./sec. The effective Reynolds number range based on pipe diameter $10^4 - 10^5$, so that flow was fully turbulent.

(ii) The number of spheres mounted, their spacing, and sphere-to-pipe diameter ratio could be varied.

(iii) Pressure drops across the spheres could be measured continuously.

(iv) There would be a high enough water pressure (up to 45 ft. of water) at the test sections not to stall the flow when sphere-to-pipe diameter ratios of up to 0.95 were used.

(v) Pressure fluctuations in the system should be minimised.

3.2 Description of Apparatus (c f. Figs. 4 - 9)

The tank (reservoir) measured 36" x 36" x 30" and was fitted with a 2½" diameter line leading to the pump; and a 1" diameter drain line. The centrifugal pump provided was rated at 3 H.P; delivering up to 100 IGPM at 50 ft. water head. It was driven by an electric motor running at 3600 rpm.

A 2" discharge line from the pump led to the Surge Chamber assembly as shown in Fig. 8a. The Surge Chamber had an effective volume of 904 cu. in. and was connected to a nitrogen bottle through a 1-in. globe valve.

Two rotameters, one covering the range 0 - 10 IGPM and the other 10 - 100 IGPM, indicated the flow rate. A butterfly valve was located between the surge chamber and flowmeters so that the flow could be regulated. Two gate valves and two globe valves for fine flow control were connected as shown in Fig. 5.

Details of the 2-in. test-sections are shown in Fig. 6. The 1-in. test-sections were identical in design except that the spacing between the sphere-location holes was $\frac{5}{8}$" and $\frac{9}{16}$" respectively; and there was an extra pressure tap provided in each test-section so that the pressure transducers could be located 3 ins. apart. A honeycomb flow-straightener was located 4 ft. from each test section. Valves downstream of the test sections enabled back pressure to be applied. (see Fig. 4.)

Two prong devices were designed and built for locating the spheres. (see Fig. 7.)

The pressure transducers are shown in Fig. 8b. The sensing element in each transducer is a stainless steel diaphram. Applied pressure varies the capacitance between the diaphram and a fixed electrode. This capacitance variation is converted into a d.c. voltage output proportional to the pressure difference between the two sides of the diaphram through the oscillator-converter arrangement described in appendix 3. The sensitivity of the pressure transducers is dependent on diaphram thickness, so four diaphrams, with thicknesses between 0.005 in. and 0.030 in., were made and fitted in the transducer units labelled PT_r3, PT_r4, PT_r1, and PT_r2; in that order of sensitivity. The pressure ranges covered by these are 0 - 30 ins. water, 0 - 10 ft. water, 10 - 30 ft. water, and 20 - 50 ft. water respectively. See Calibration curves (Appendix 1).

There were difficulties in getting the equipment designed and the instruments calibrated and working properly, but these were eventually solved.

3.3. Experimental Procedure

The converter units were switched on to warm up, at least 1 hr. before the start of each experiment. This minimised drift.

The reservoir was filled with water to ½ capacity and the pump stuffing box nuts (2 off) were adjusted so that there was slight drip of water as the driving-shaft was rotated slowly by hand. This indicated that the pump was well primed.

Spheres were located in the appropriate test-section using the prong devices mentioned above; and the test-section was fitted into place by bolting the Johnson dresser couplings provided.

The appropriate transducers were adjusted so that the output voltages were zero, and the valves in the system were checked to ensure that the right ones were open and the others closed. Care was taken that the flow rate which was obtained did not exceed the range of the smaller flowmeter when that rotameter was used.

Care was also taken that the output of the pressure transducers did not exceed 6 volts d.c.

The readings of voltage were taken from the recorder, and millimeter readings of the rotameters were also noted as flow rate was varied. Water temperature was measured using a mercury thermometer. Since the variation of water temperature throughout any experiment was less than 3%, water temperatures were taken only at the beginning and at the end of each experiment.

Using calibration charts, values of the flow rate, pressure drop, and Reynolds numbers were calculated from the readings listed above.

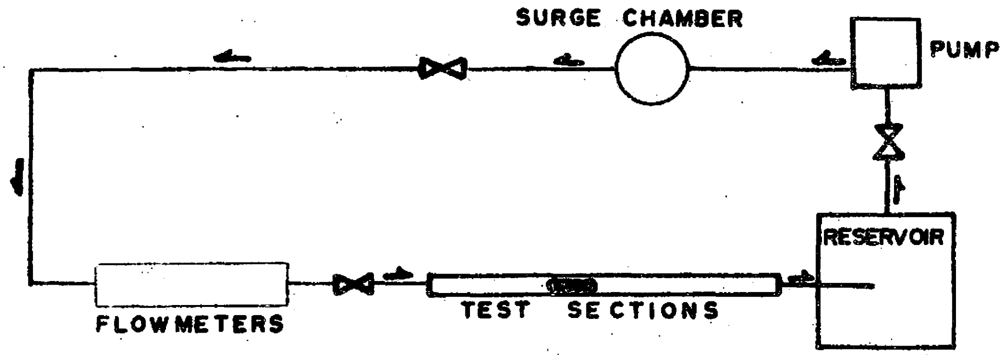

PLAN

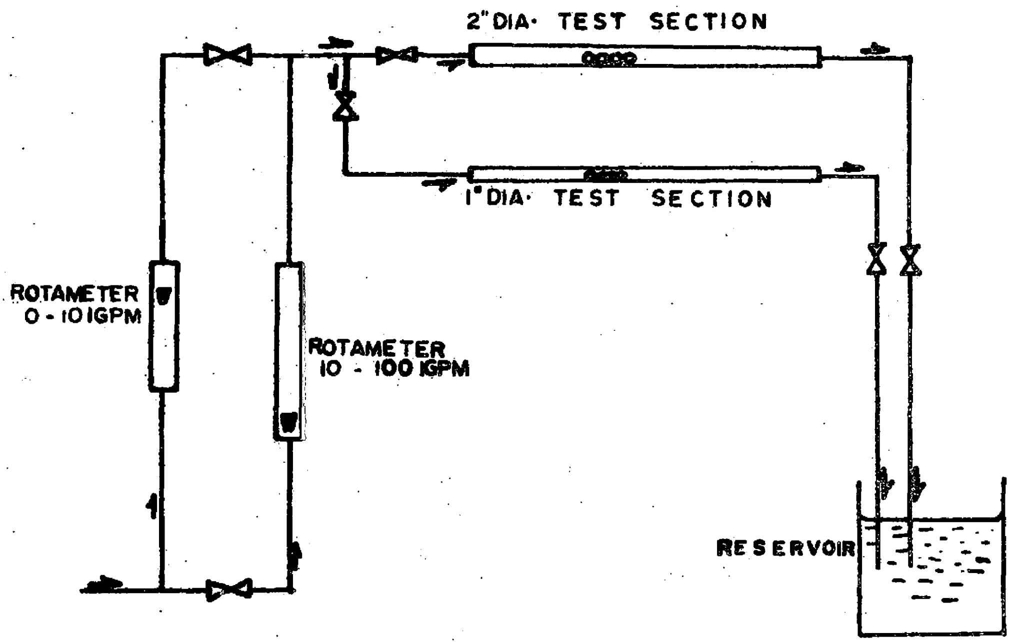

FIGURE NO. 4

SCHEMATIC DIAGRAMS OF THE APPARATUS

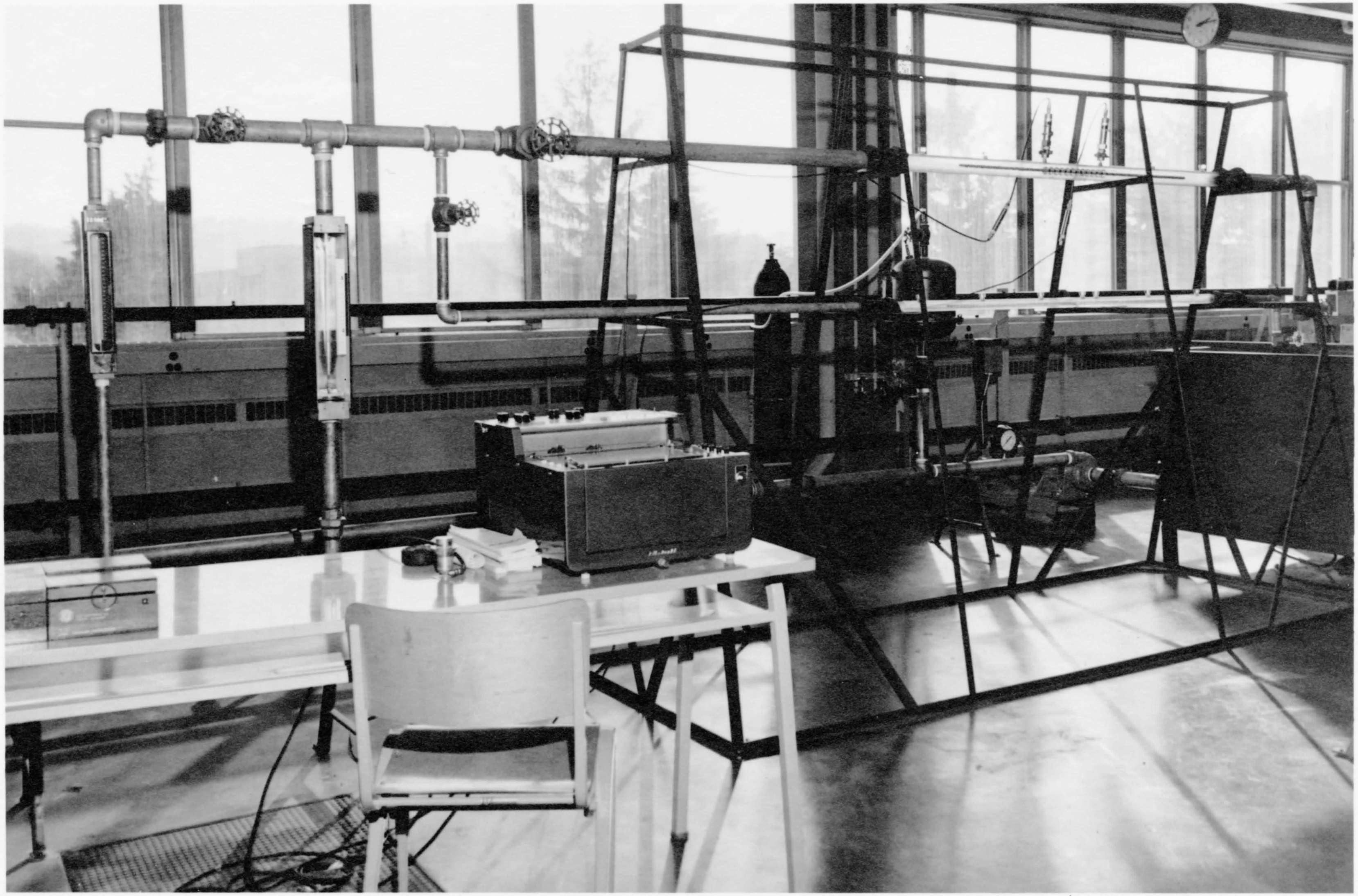

FIG. 5 - GENERAL VIEW OF THE EQUIPMENT

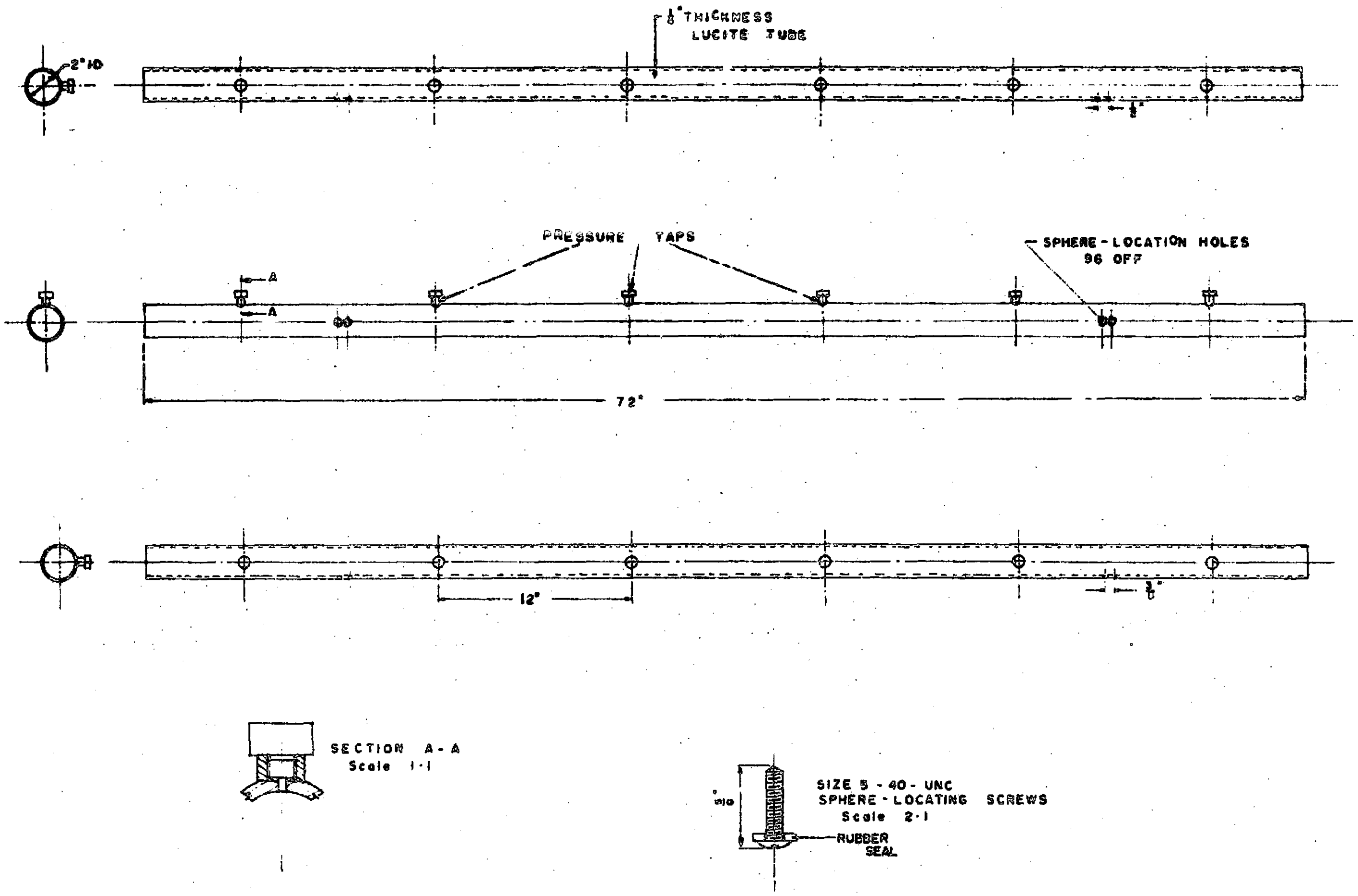

FIGURE NO. 6

DETAILS OF THE TEST SECTIONS

FIG. 7 - SPHERE-LOCATING TOOLS

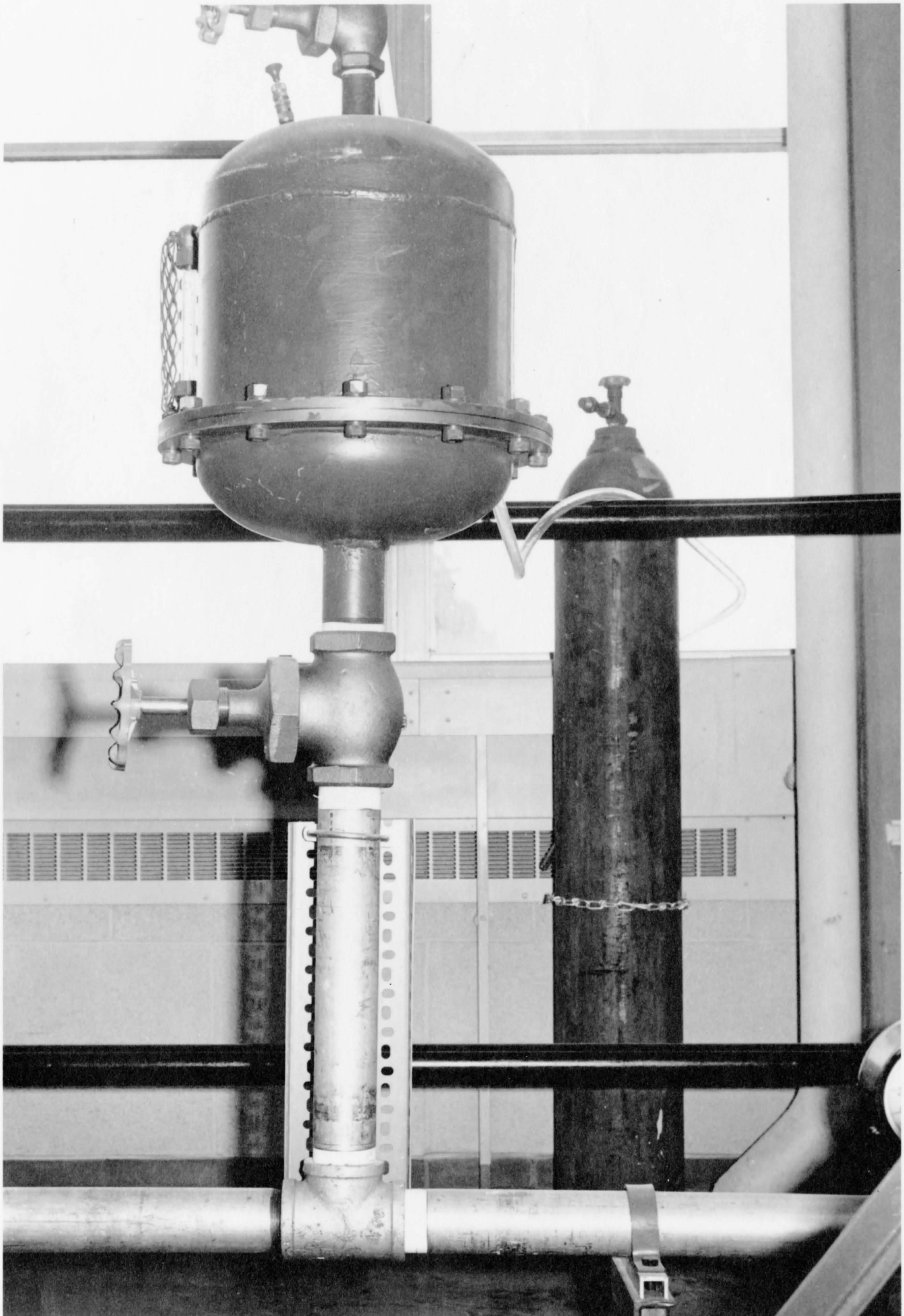

FIG. 8a - SURGE CHAMBER ASSEMBLY

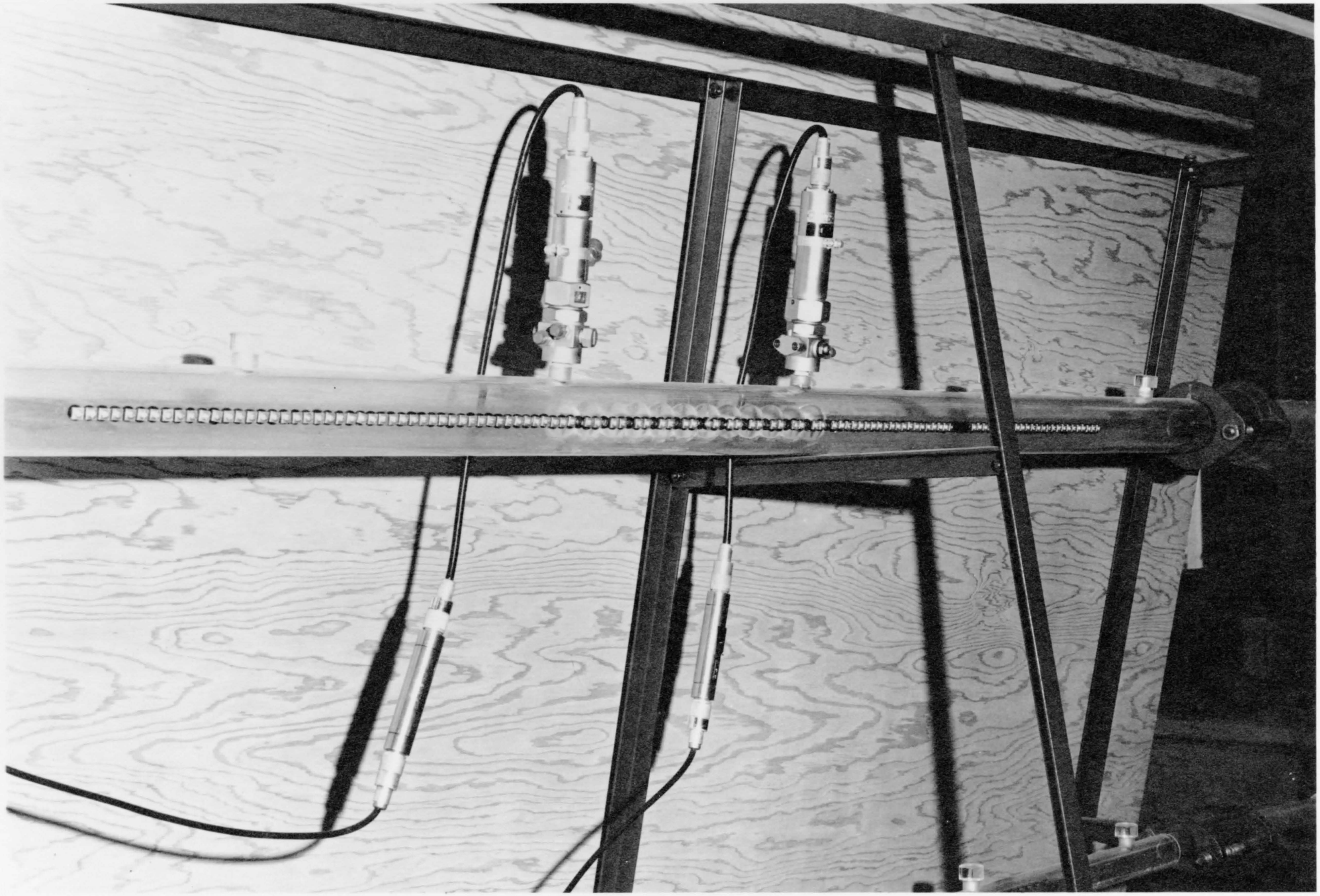

FIG. 8b - PRESSURE TRANSDUCERS ASSEMBLY

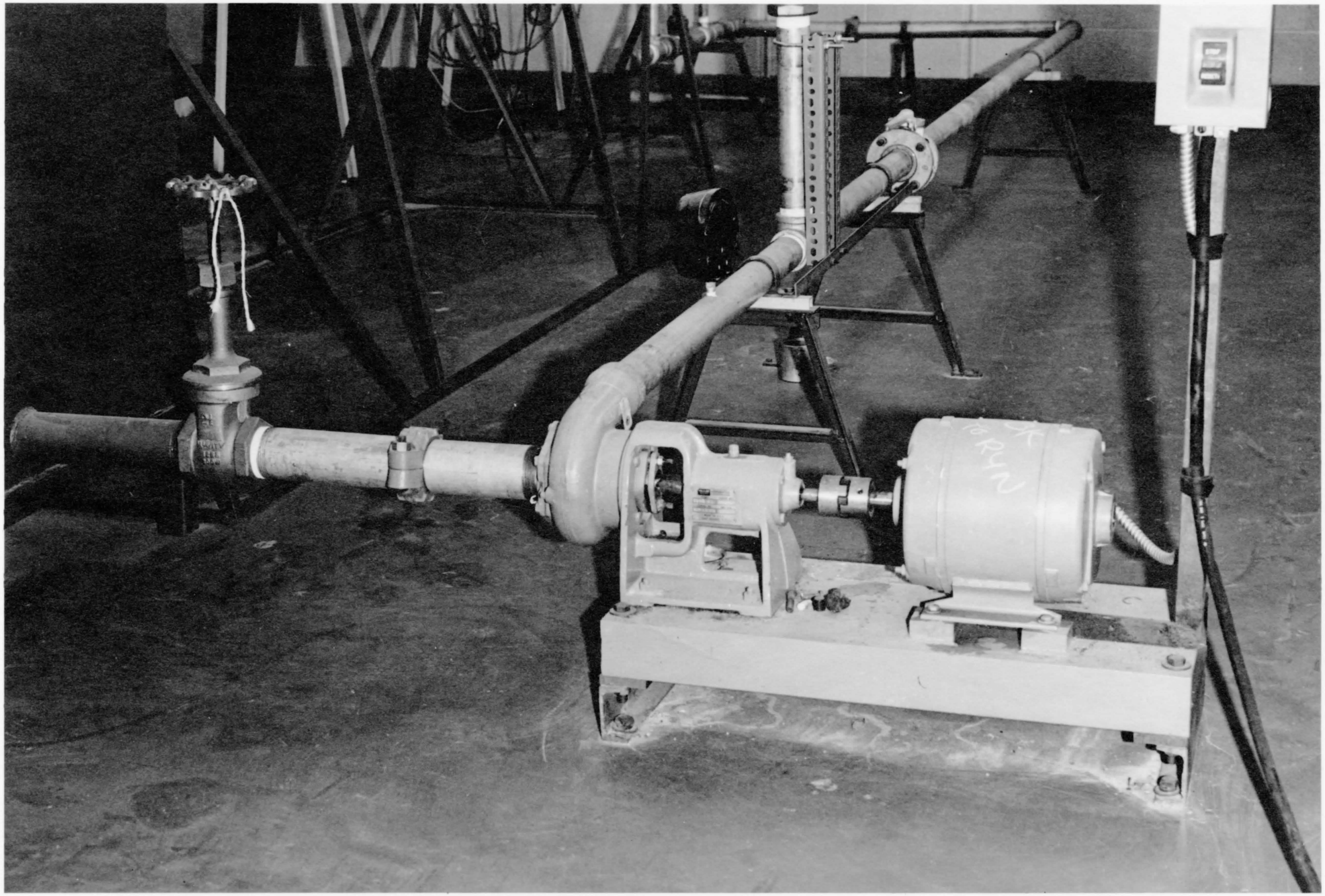

FIG. 8c - THE PUMP AND PIPING ARRANGEMENT

4. RESULTS AND CALCULATIONS

The experiments were conducted using the following series of spheres:-

1" diameter spheres in 2" pipe (diam. ratio = 0.486);
⅝" spheres in 1" pipe (diam. ratio = 0.60);
1½" spheres in 2" pipe (diam. ratio = 0.737); and
⅞" spheres in 1" pipe (diam. ratio = 0.84).

The internal diameter of each pipe (test section) was measured and found to be 1.030 ± 0.010 in. and 2.000 ± .010 in. respectively.

For each diameter ratio, tests were performed, as described in section 3.3 with 1 sphere, 2 spheres, 4 spheres, 8 spheres, and 12 (or 10) spheres located in the pipe. Calculations of the basic parameters - pressure drop and Reynolds number - were made from readings of the flow rate, transducer voltage output and temperature as follows:

$$\text{Pressure Drop} = Vo_1\, C_1 - Vo_2\, C_2$$

where Vo_1 was the upstream transducer voltage output, C_1 was the calibration constant for the upstream pressure transducer, and suffix 2 refers to the downstream pressure transducer. The values of C_1 and C_2 depended on which of the four transducers - PT_r1, PT_r2, PT_r3, PT_r4 - were used; and were obtainable from the calibration charts. See Fig. 9

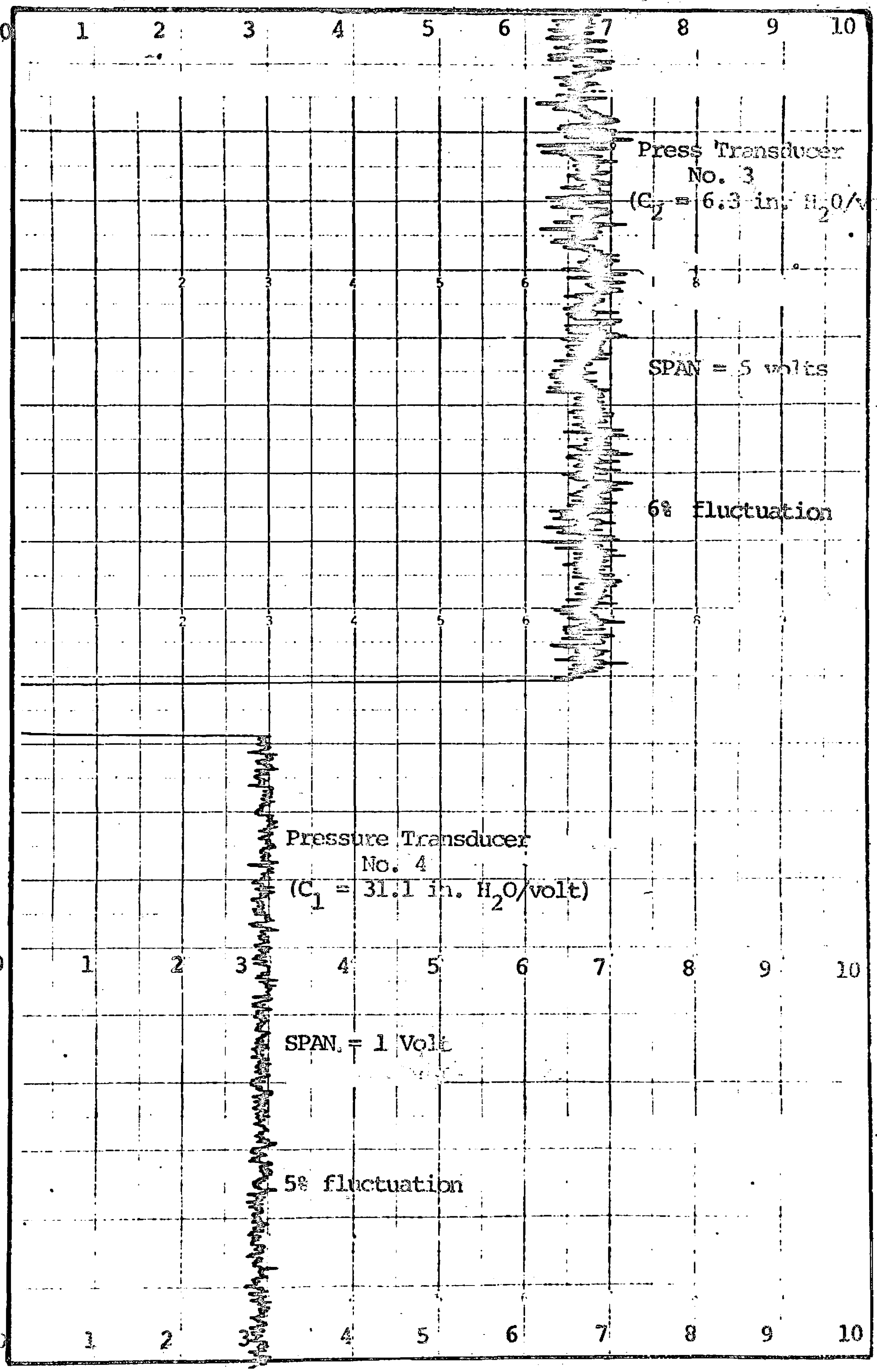

Fig. 9 TYPICAL RECORDER TRACES

Reynolds number (based on pipe diam.) = $0.04083(\frac{Q}{\nu_t D})$ (4.1)

where Q is the flow rate in Imperial gal./min., D is the pipe internal diameter in in. and ν_t is the kinematic viscosity of water (in ft^2/sec.) at the temperature measured. The values of kinematic viscosity were obtained from tables. (See appendix 1 for the derivation of equation (4.1).)

Having obtained the pressure drops and corresponding Reynolds numbers, the parameters developed in Chapter 2 were evaluated. The correlation of these parameters is presented below and will be further discussed in the next chapter.

4.1 'N-sphere' system: PR1 as a function of Reynolds Number and Diameter Ratio.

Data collected with the 'n-sphere' system (cf. Fig. 1, Case D) were used to compute the parameter PR1 defined by equations (2.4.1) and (2.1.3). (The computer program output is given in appendix 4.) The data are given in table No. 5.

Contrary to the simple analysis of section 2.4, PR1 was not completely independent of Reynolds number, as shown in Fig. 10. The maximum variation of PR1 with Reynolds number occured with the sphere/pipe diameter ratio of 0.84. The minimum variation was found with the 0.60 and 0.737 diameter ratios.

The values of PR1 given by equation (2.4.8) were compared with those computed from data. Discrepancies of about 100 % or more were observed between the two sets of PR1. This suggests that the simple analysis of section 2.4, based on the equivalent diameter concept, is inadequate for the complex flow phenomena within the corrugated annuli.

Correlating the values of PR1 at a Reynolds number of 10,000, an empirical formula for PR1 as a function of diameter ratio was obtained:

$$PR1 = 259.133 \cdot \left(\frac{d}{D}\right)^{4.543} \qquad (4.2)$$

Considering equation (4.2) and the variation of the pressure ratio, PR1, with Reynolds number, a more general formula was derived:

$$PR1 = \left[259.133 \cdot \left(\frac{d}{D}\right)^{4.543}\right] R_e'^{\,c} \qquad (4.3)$$

where $c = 0.232$, for $\frac{d}{D} = 0.486$ $\quad R_e' = 10^{-4} \cdot R_e$

$c = 0.074$, for $\frac{d}{D} = 0.6$

$c = 0.082$, for $\frac{d}{D} = 0.737$

and $c = 0.33$, for $\frac{d}{D} = 0.84$

That is, c varied between 0 and 0.33 for the range of diameter ratios and Reynolds numbers considered. It will be seen from the plot of PR1 vs. R_e that the mean value of PR1 for each diameter ratio corresponds to a Reynolds number between 3×10^4 and 4×10^4. Fig. 11 therefore applies more accurately to Reynolds numbers within that range.

4.2 Measurements including end effects (cf. Fig. 1 case A,B & C)

(i) Pressure Gradient based on length of the sphere train, n.d.

The parameter $(\frac{dp}{dz})_{corr}$, defined in equation (2.3.2) was calculated from the data given in tables 1 - 4. It is a function of Reynolds number, diameter ratio, and number of spheres; and has been plotted for each of the four diameter ratios as shown in Fig. 12.

All the plots are linear on a log-log scale. The gradients vary between 1.5 and 2.0, with the exception of the smallest diameter ratio where lesser gradients were observed. From the plots, the following general observations were made:

(a) DPZC $\left(\text{i.e. } (\frac{dp}{dz})_{corr.}\right)$ increases with increase of Reynolds number

(b) For a given pipe diameter and number of spheres, DPZC increases with increase in diameter ratio

(c) For diameter ratios of 0.6 and 0.737, DPZC decreased steadily with increase in number of spheres. An oscillating decrease in DPZC was however observed with the 0.486 and 0.84 diameter ratios as the number of spheres increased.

(ii) End effect (on pressure gradient) as a function of Reynolds Number, Diameter Ratio, and number of spheres.

From equation (2.3.6) the end-effect component of pressure gradient was computed and the results plotted as shown in Fig.13. Like the DPZC versus R_e plots the end effect graphs were linear on a log-log scale with the exception of the 0.486 diam. ratio plot, where some nonlinearities were observed. The following general observations are made:-

(a) The end-effect component of pressure gradient tends to decrease as the number of spheres in the train increases. It decreases from 100 % of DPZC (total pressure gradient) for 1 sphere, to between 20 % and 60 % DPZC for 12 spheres, depending on the diameter ratio. The respective lower limits of end effect computed were 58.7 % for $(\frac{d}{D}) = 0.486$; 40.9 % for $(\frac{d}{D}) = 0.60$; 23 % for $(\frac{d}{D}) = 0.737$; and 48.2 % for $(\frac{d}{D}) = 0.84$.

(b) The end effects generally increased with increase of Reynolds number and sphere-to-pipe diam. ratio for any given pipe diameter.

(iii) <u>PR2 as a function of R_{e_N}, No. of spheres, and Diameter ratio.</u>

The pressure ratio PR2, is defined in equation (2.4.9). Figs. 14 and 15 illustrate the variation of PR2 with Reynolds number and number of spheres in the train. PR2 tends to decrease with increase in diameter ratio for a given number of spheres amd a given Reynolds number.

(iv) <u>Pressure gradient based on length, L, between pressure taps.</u>

Equation (2.3.2) can be written in the form

$$\left[\left(\frac{P_1-P_2}{L}\right) - \left(\frac{dp}{dz}\right)_n (n-1)\frac{d}{L}\right] \left(\equiv \text{DPZCL}\right)$$

$$= \left(\frac{dp}{dz}\right)_{LIQ} \left[\frac{L - (n-1)d}{L} + f\left(\frac{d}{D}, R_{e_N}, n\right)\right]$$

where $f\left(\frac{d}{D}, R_{e_N}, n\right)$ is directly dependent on the end effects.

To check the validity of equation (2.3.2), and hence the results presented above, DPZCL was computed and plotted against $\left(\frac{dp}{dz}\right)_{LIQ}$ using all the data. For the results to be valid, the graphs of DPZCL versus $\left(\frac{dp}{dz}\right)_{LIQ}$ must pass through the origin and with gradients reflecting the end effects. As shown in Fig. 16 the graphs of DPZCL versus $\left(\frac{dp}{dz}\right)_{LIQ}$ pass through the origin.

4.3 Drag Coefficient

From equation (2.5.5) and (2.5.6) the drag coefficients were evaluated for the diameter ratio of 0.84 using pressure drop measurements. Values of drag coefficient calculated from pressure drop data were higher than those corresponding to the theoretical formula,

$$C_D = \left[\left(\frac{d}{D}\right)/1 - \left(\frac{d}{D}\right)^2\right]^2$$

The best agreement between the latter values and the former was at pipe-Reynolds-numbers greater than 8.5×10^4. The corresponding discrepancy was less than 10 %. See Fig. 17.

4.4 Error Analysis

The following analysis is based on estimates of error due to such factors as instrument error, calibration error, reading error, errors in measurement of the length and diameter of test-sections, and manufacturer's quotation.

Pressure drop measurement:	Max.	error	estimated	=	± 7 %
Flow rate measurement :	"	"	"	=	± 6 %
Length, L, between transducers :	"	"	"	=	± 0.5 %
Mean diameter, D, of test section :	"	"	"	=	± 1.0 %
Kinematic viscosity (with temperature measurement :	"	"	"	=	± 2.0 %
Sphere diameter measurement :	"	"	"	=	± 1.0 %

(i) Reynolds number - calculated from equation (4.1).

$\therefore$ Max. error in R_{e_N} = % error in Q + % error in ν + % error in D = (6 + 2 + 1)% = ± 9 %

(ii) Pressure gradient, $\left(\frac{dp}{dz}\right)_n = \left(\frac{P1n-P2n}{L}\right)$

$\therefore$ Max. error in DPZN = error in pressure drop + error in L measurement.

= ± (7 + 0.5)%

= ± 7.5 %

(iii) Free pipe pressure gradient, $\left(\frac{dp}{dz}\right)_{LIQ}$ - calculated from equation (2.1.3).

$\therefore$ Max. error in DPZL = 2 x error in kinem. viscosity + 1.75 x error in Re_N + 3 x error in D

$= \pm(4 + 16 + 3)\% = 23\ \%$

(iv) Pressure gradient (DPZC) based on the length of the sphere train - defined in equation (2.3.2).

Error in DPZC = Error in pressure drop measurement + error in sphere diameter

$= \pm(7 + 1)\% = \pm\ 8\ \%$

(v) Pressure Ratio, $PR1 = \dfrac{\left(\frac{dp}{dz}\right)_n}{\left(\frac{dp}{dz}\right)_{LIQ}}$

$\therefore$ Max. error in PR1 = Max. error in $\left(\frac{dp}{dz}\right)_n$ + Max. error in $\left(\frac{dp}{dz}\right)_{LIQ}$

$= \pm(7.5 + 23)\% = 31\ \%$

(vi) Pressure ratio, $PR2 = \dfrac{DPZC}{DPZN}$

$\therefore$ Max. error in PR2 = Max. error in DPZC + Max. error in DPZN

$= \pm(8 + 7.5)\%$

$= \pm\ 16\ \%$

(vii) Drag coefficient, $C_D = \dfrac{D^2}{d^2} \cdot \left[\dfrac{\text{Pressure Drop}}{Vo^2/2g}\right]$

where $V_O = \dfrac{\nu\ .\ Re_N}{D} \times 14.4$

Error in Vo = 2 + 9 + 1 = ± 11 %

Max. Error in C_D = 2(2) + 7 + 22 = 33 %

4.5 Application of the results

The essence of the non-dimensional parameters, PR1 and PR2, was to generalize the results of this experimental study so that they may be applicable to any pipe diameter and for any sphere-pipe diameter ratio between 0.486 and 0.85; the Reynolds number range being $10^4 - 10^5$. We shall illustrate in this section how the results can be applied to predict the pressure drop in an arbitrary pipe of diameter, D (say 6 in.) with n (say 100) spheres of diameter d (say 4½ ins.) located in the pipe as water flows past them with a mean velocity Vo (say 1 ft/sec.) at a temperature, T (say 74 F, i.e. kinematic viscosity = 1.0×10^{-5} ft^2/sec.).
The following procedure is recommended:-

(a) Calculate the Reynolds number based on pipe internal diameter, knowing the kinematic viscosity corresponding to the temperature, T.

(b) Calculate the free-pipe pressure gradient, $\left(\frac{dp}{dz}\right)_{LIQ}$ using the equation

$$\left(\frac{dp}{dz}\right)_{LIQ} = 8.487 \left(\frac{\nu^2 \,.\, Re_N^{1.75}}{D^3}\right)$$

where D is in inches and ν is in ft^2/sec.

(c) If the length, L, between pressure measurement points along the pipe is less or equal to the total length of the sphere train, then we require the parameter PR1 only. If L is greater than the total length of the sphere train, we require both PR1 and PR2.

(i) Suppose L is less or equal to n.d. Referring to Fig. 10, the value of PR1 corresponding to the given sphere-to-pipe diameter ratio and Reynolds number is read off. Interpolate if necessary.

Now, $PR1 = \dfrac{\Delta P}{L\left(\frac{dp}{dz}\right)_{LIQ}}$

where ΔP is the pressure drop in inches water required, and L is also in inches. Knowing $\left(\frac{dp}{dz}\right)_{LIQ}$, L and PR1, we thus predict the pressure drop.

Equation (4.3) could also be applied to calculate PR1.

(ii) If L is greater than n.d, we use Fig. 14. Depending on the number of spheres in the train, the value of PR2 is read off corresponding to the diameter ratio and Reynolds number calculated above. Where the number of spheres is very large (say 50 or more spheres) a conservative estimate of pressure drop can be obtained by reading off PR2 from the lowest graph corresponding to the given diameter ratio.

$$\text{Now, } PR2 = \frac{\Delta P - \left(\frac{dp}{dz}\right)_{LIQ} \left(L-(n-1)d\right)}{n \times d \times \left(PR1 \times \left(\frac{dp}{dz}\right)_{LIQ}\right)}$$

where ΔP is the pressure drop required, and $\left(\frac{dp}{dz}\right)_{LIQ}$ and PR1 are evaluated as indicated above.

Substituting, therefore, we obtain ΔP.

For example, using the figures given above, let L = 500 ins.

$$\text{Reynolds number} = \frac{1.0 \times \frac{1}{2}}{1} \times 10^5 = 5.0 \times 10^4$$

$$\left(\frac{dp}{dz}\right)_{LIQ} = \frac{8\text{-}487 \times 5^{1.75}}{6^3} \times 10^{-3}$$ inches water per inch length of pipe.

$$= .000654$$

We note that L > 100 x 4.5, so we require both parameters, PR1 and PR2. Diameter ratio = 0.75. So we interpolate between 0.737 and 0.84. From Fig. 11 we read that PR1 = 90.0 approximately at the Reynolds number of 5×10^4 and $\frac{d}{D} = 0.75$. From Fig. 14 we take PR2 = 1.2 for the given number of spheres and Reynolds number.

Substituting in equation (4.4),

$$1.2 = \frac{\Delta P - 6.54 \times 10^{-4} (500 - 445.5)}{100 \times 4.5 \times 9 \times 6.5 \times 10^{-4}}$$

$$\therefore \Delta P = 1.2 \times 4.5 \times 9 \times 6.54 \times 10^{-2} + 6.54 \times 54.5 \times 10^{-4}$$

$$= 3.18 + 0.0357 = 3.216$$

$\therefore$ Pressure drop expected = 3.2 ins. water

We have thus predicted the pressure drop corresponding to the data chosen arbitrarily above.

4.6 Optimum Diameter Ratio For Sphere Trains

The power consumption per unit mass flow rate is given as:

$$\frac{\text{H.P./ft}}{(\text{tons/sec})} = \beta \frac{\text{PRI}}{(\frac{d}{D})^2} \qquad (5.5.1)$$

where β is a constant

See appendix 2 for the derivation of equation 5.5.1. Using figure 11 the above parameter can be calculated and tabulated as follows:

$(\frac{d}{D})$	PRI	$\frac{\text{HP/ft}}{\text{tons/sec}} \cdot \frac{1}{\beta}$
1.0	∞	∞
0	1	∞
0.4	10.5	65.6
0.45	12	59.3
0.5	14.5	58.0
0.55	18	59.5
0.6	23	63.9
0.7	52	106.1
0.8	150	234.4

The minimum power consumption for a given solids through put thus corresponds to a sphere/pipe diameter ratio of 0.5.

TABLE NO.1

DATA FOR 2" DIA. PIPE $\frac{d}{D} = 0.486$

1 Sphere	L = 12 ins. Kinem. Viscosity =0.96 ft^2/sec. ($\times 10^{-5}$)										
$R_{e_N} \times 10^{-4}$	1.99	2.71	3.42	4.94	5.72	6.53	7.33	7.33	8.17	9.19	10.1
Press.Drop (ins.water)	1.4	2.2	1.6	1.6	2.0	2.5	2.9	2.9	3.1	3.4	4.25
2 Spheres	L = 60 ins. Kinem. Viscosity =0.94 ft^2/sec. $\times 10^{-5}$										
$R_{e_N} \times 10^{-4}$	2.1	2.88	4.45	4.45	6.1	6.1	7.8	7.8	9.7	9.7	10.7
Press.Drop (ins.water)	3.7	3.5	4.1	4.1	6.7	6.7	7.1	7.1	9.0	9.0	9.2
4 Spheres	L = 12 ins. Kinem. Viscosity =0.95 ft^2/sec. $\times 10^{-5}$										
$R_{e_N} \times 10^{-4}$	2.1	2.9	3.6	5.2	6.0	6.9	8.6	8.6	9.7	9.7	10.6
Press.Drop (ins.water)	1.8	2.5	3.8	3.5	4.1	4.7	5.6	5.6	7.0	7.0	8.1
8 Spheres	L = 60 ins. Kinem. Viscosity = 1.0 ft^2/sec. $\times 10^{-5}$										
$R_{e_N} \times 10^{-4}$	1.99	2.71	4.19	5.72	6.5	7.33	8.2	8.2	9.19	9.19	10.1
Press.Drop (ins.water)	1.76	1.6	2.53	4.2	6.6	8.1	10.8	10.8	13.8	13.8	16.6
12 Spheres	L = 60 ins. Kinem. Viscosity =1.08 ft^2/sec. $\times 10^{-5}$										
$R_{e_N} \times 10^{-4}$	1.85	2.52	3.18	3.9	4.6	5.3	6.07	6.8	7.6	8.5	9.35
Press.Drop (ins.water)	1.85	2.4	5.66	8.7	9.6	10.5	13.4	15.0	18.0	21.0	24.8

TABLE NO.2

DATA FOR 1" DIA. PIPE $\frac{d}{D} = 0.60$

1 Sphere	L = 9 ins. Kinem. Viscosity $= 0.95\ ft^2/sec. \times 10^{-5}$										
$R_{e_N} \times 10^{-4}$	1.42	2.11	2.57	2.82	3.04	3.6	3.8	4.06	4.64	5.21	5.5
Press.Drop (ins.water)	1.4	1.8	2.8	2.6	3.35	4.1	5.5	5.4	6.9	8.0	9.1
2 Spheres	L = 3 ins. Kinem. Viscosity $= 0.95\ ft^2/sec. \times 10^{-5}$										
$R_{e_N} \times 10^{-4}$	1.47	2.06	2.7	4.37	5.5	6.64	7.2	7.79	8.37	8.96	9.53
Press.Drop (ins.water)	1.6	3.2	4.4	6.58	10.4	15.0	18.0	20.6	23.0	28.5	31.8
4 Spheres	L = 3 ins. Kinem. Viscosity $= 0.95\ ft^2/sec. \times 10^{-5}$										
$R_{e_N} \times 10^{-4}$	1.47	2.7	3.78	4.37	4.94	5.5	6.07	7.2	8.37	8.96	9.5
Press.Drop (ins.water)	1.1	3.4	8.2	9.4	12.0	15.9	19.3	26.4	35.2	39.2	45.7
8 Spheres	L = 48 ins. Kinem. Viscosity $= .875\ ft^2/sec. \times 10^{-5}$										
$R_{e_N} \times 10^{-4}$	4.07	4.71	5.3	5.93	6.55	7.2	7.79	8.4	9.02	9.65	10.3
Press.Drop (ins.water)	14.1	18.8	25.2	32.2	37.5	44.7	51.8	61.5	70.0	76.7	89.6
12 Spheres	L = 48 ins. Kinem. Viscosity $= 0.90\ ft^2/sec. \times 10^{-5}$										
$R_{e_N} \times 10^{-4}$	3.96	4.57	5.17	5.76	6.36	6.95	7.57	8.16	8.76	9.37	9.96
Press.Drop (ins.water)	19.3	26.0	35.7	41.2	51.0	61.9	72.4	85.3	97.9	111.0	124.0

TABLE NO. 3

DATA FOR 2" DIA. PIPE $\frac{d}{D} = 0.737$

1 Sphere	L = 12 ins. Kinem. Viscosity = 0.95 $ft^2/sec. \times 10^{-5}$										
$R_{e_N} \times 10^{-4}$	2.1	2.85	3.6	4.41	5.2	6.02	6.88	7.7	8.6	9.65	10.6
Press.Drop (ins.water)	0.90	3.0	4.4	4.4	6.0	7.4	9.8	11.2	12.7	14.9	16.6
2 Spheres	L = 60 ins. Kinem. Viscosity = 0.90 $ft^2/sec. \times 10^{-5}$										
$R_{e_N} \times 10^{-4}$	2.2	3.0	3.8	4.7	5.5	6.4	7.26	8.1	9.08	10.2	11.2
Press.Drop (ins.water)	0.7	3.5	2.9	5.2	6.0	8,6	10.8	13.0	16.1	20.2	25.9
4 Spheres	L = 12 ins. Kinem. Viscosity = .875 $ft^2/sec. \times 10^{-5}$										
$R_{e_N} \times 10^{-4}$	2.28	3.1	3.9	4.8	5.6	6.5	7.46	8.36	9.3	10.5	11.5
Press.Drop (ins.water)	2.80	2.80	4.6	6.4	9.2	12.2	16.8	20.8	27.0	32.6	39.1
10 Spheres	L = 36 ins. Kinem. Viscosity = .923 $ft^2/sec. \times 10^{-5}$										
$R_{e_N} \times 10^{-4}$	2.16	2.93	3.7	4.53	5.35	6.19	7.07	7.9	8.84	9.92	10.9
Press.Drop (ins.water)	4.8	7.8	11.8	16.7	22.5	29.7	38.4	49.9	61.6	75.3	91.3
Spheres	L = ins. Kinem. Viscosity = $ft^2/sec. \times 10^{-5}$										
$R_{e_N} \times 10^{-4}$											
Press.Drop (ins.water)											

TABLE NO. 4

DATA FOR 1" DIA. PIPE $\frac{d}{D} = 0.84$

1 Sphere	L = 9 ins. Kinem. Viscosity = 0.95 $ft^2/sec. \times 10^{-5}$										
$R_{e_N} \times 10^{-4}$	1.48	2.06	3.20	4.38	4.93	5.52	9.07	8.5	7.96	6.88	6.32
Press.Drop (ins.water)	5.3	8.4	17.7	32.7	40.6	50.2	118	107	99.9	80.0	68.5
2 Spheres	L = 9 ins. Kinem. Viscosity = 0.93 $ft^2/sec. \times 10^{-5}$										
$R_{e_N} \times 10^{-4}$	10.3	9.7	8.56	7.40	6.79	6.2	5.1	5.1	4.47	3.87	3.27
Press.Drop (ins.water)	156	159	130	99.2	84.0	69.7	46.0	46.0	36.2	28.0	20.6
4 Spheres	L = 9 ins. Kinem. Viscosity = .925 $ft^2/sec. \times 10^{-5}$										
$R_{e_N} \times 10^{-4}$	1.5	2.71	3.27	3.87	5.05	5.6	6.79	7.98	8.56	9.16	9.74
Press.Drop (ins.water)	8.1	22.1	32.1	45.4	76.2	97.1	142	173	183	181	177
8 Spheres	L = 48 ins. Kinem. Viscosity = 0.91 $ft^2/sec. \times 10^{-5}$										
$R_{e_N} \times 10^{-4}$	3.9	4.5	4.5	5.1	5.1	5.7	5.7	6.3	6.89	7.5	8.09
Press.Drop (ins.water)	112	152	152	195	195	246	246	295	345	397	452
12 Spheres	L = 48 ins. Kinem. Viscosity = .925 $ft^2/sec. \times 10^{-5}$										
$R_{e_N} \times 10^{-4}$	3.24	3.85	3.85	4.4	4.4	5.0	5.0	5.6	5.6	6.2	6.2
Press.Drop (ins.water)	134	196	196	266	266	346	346	417	417	502	502

TABLE NO. 5

'N-SPHERE SYSTEMS' DATA

$\frac{d}{D} = 0.486$ 12 Spheres	L = 12 ins. Kinem. Viscosity = .923 $ft^2/sec. \times 10^{-5}$											
$R_{e_N} \times 10^{-4}$	3.7	3.7	5.35	6.19	6.19	7.07	7.93	8.84	8.84	9.92	10.88	2" PIPE
Press.Drop (ins.water)	1.7	1.7	2.2	4.7	4.7	5.3	7.9	9.7	9.7	10.0	13.1	
$\frac{d}{D} = 0.60$ 8 Spheres	L = 3 ins. Kinem. Viscosity = 0.95 $ft^2/sec. \times 10^{-5}$											
$R_{e_N} \times 10^{-4}$	1.45	2.6	3.14	4.29	5.41	6.53	7.66	8.22	8.80	9.35	9.91	1" PIPE
Press.Drop (ins.water)	1.0	2.30	3.5	5.3	7.8	12.7	17.2	20.8	22.9	27.7	32.7	
$\frac{d}{D} = 0.737$ 10 Spheres	L = 12 ins. Kinem. Viscosity = 0.88 $ft^2/sec. \times 10^{-5}$											
$R_{e_N} \times 10^{-4}$	2.3	3.1	3.9	4.8	5.6	6.5	7.4	8.3	9.3	10.4	11.4	2" PIPE
Press.Drop (ins.water)	3.6	5.2	8.7	12.4	15.7	21.6	27.3	35.7	44.3	55.7	63.2	
$\frac{d}{D} = 0.85$ 12 Spheres	L = 9 ins. Kinem. Viscosity = .925 $ft^2/sec. \times 10^{-5}$											
$R_{e_N} \times 10^{-4}$	0.95	1.5	2.1	2.7	3.3	3.9	4.5	5.1	5.6	6.2	6.8	1" PIPE
Press.Drop (ins.water)	6.9	20.3	28.4	47.3	73.5	142	187	247	310	297	353	
Spheres	L = ins. Kinem. Viscosity = $ft^2/sec.$											
$R_{e_N} \times 10^{-4}$												
Press.Drop (ins.water)												

Fig. 10

PRESSURE RATIO, PR1, VERSUS R_e

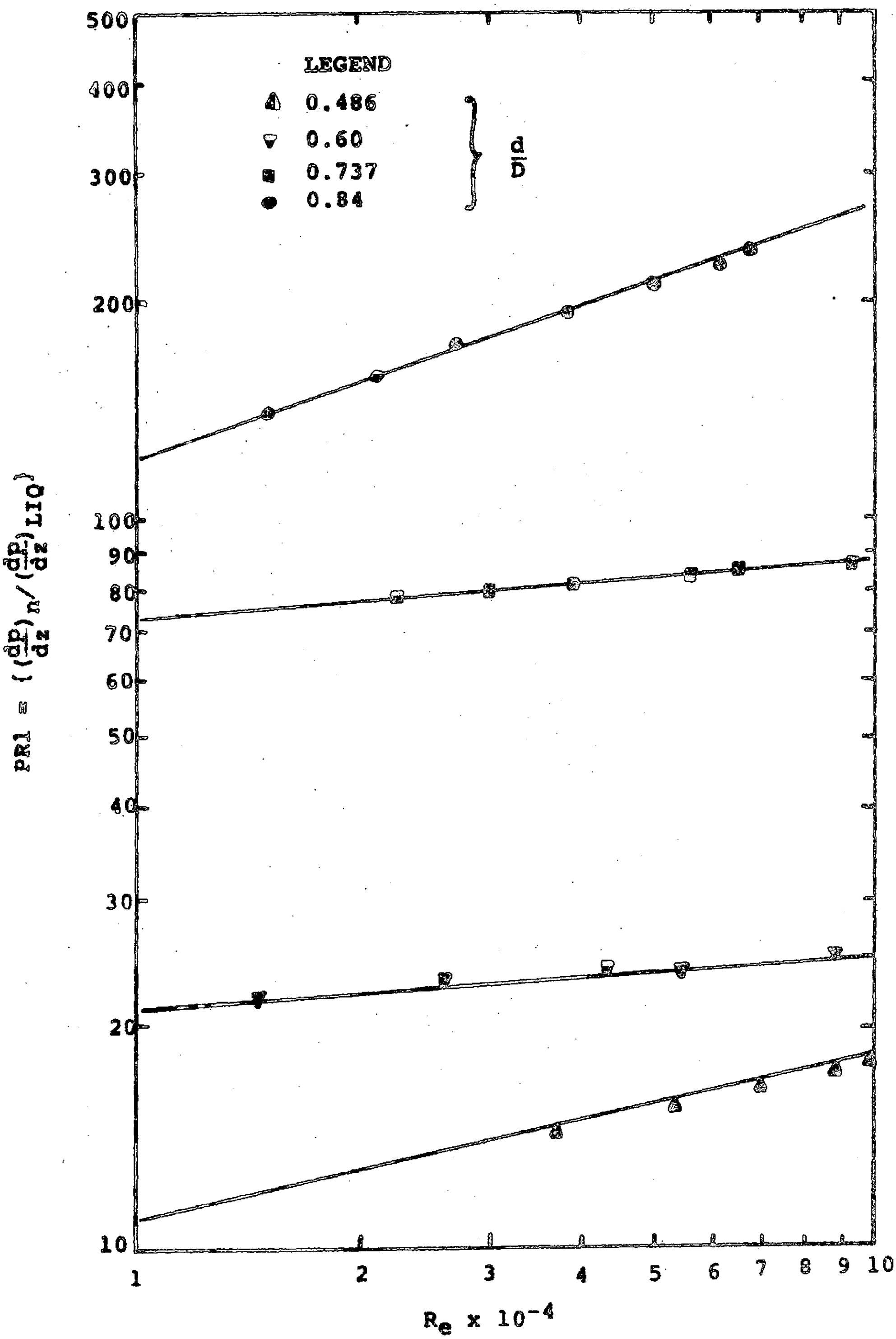

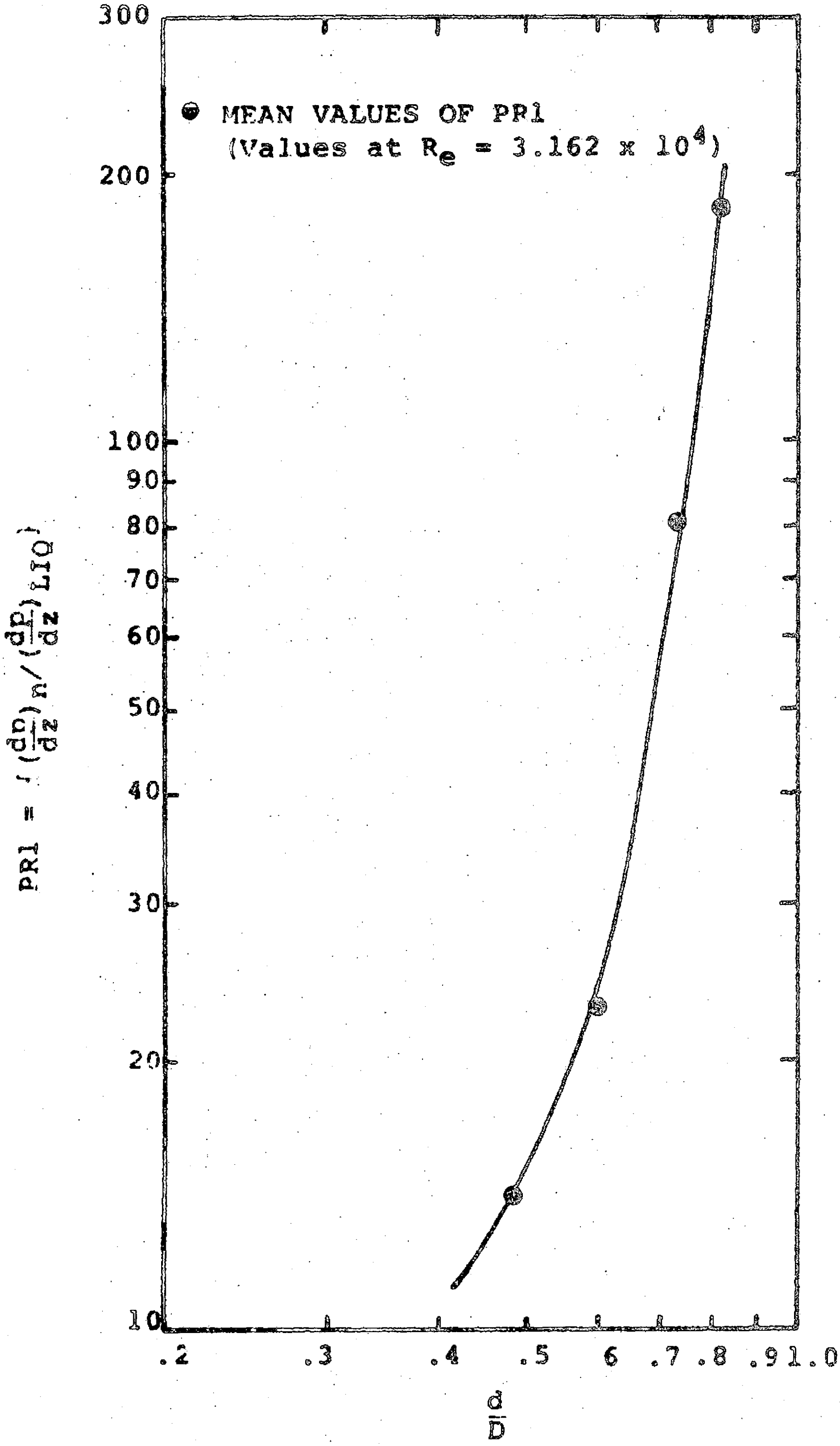

Fig. 11 PRESSURE RATIO, PR1, VERSUS DIAM.RATIO

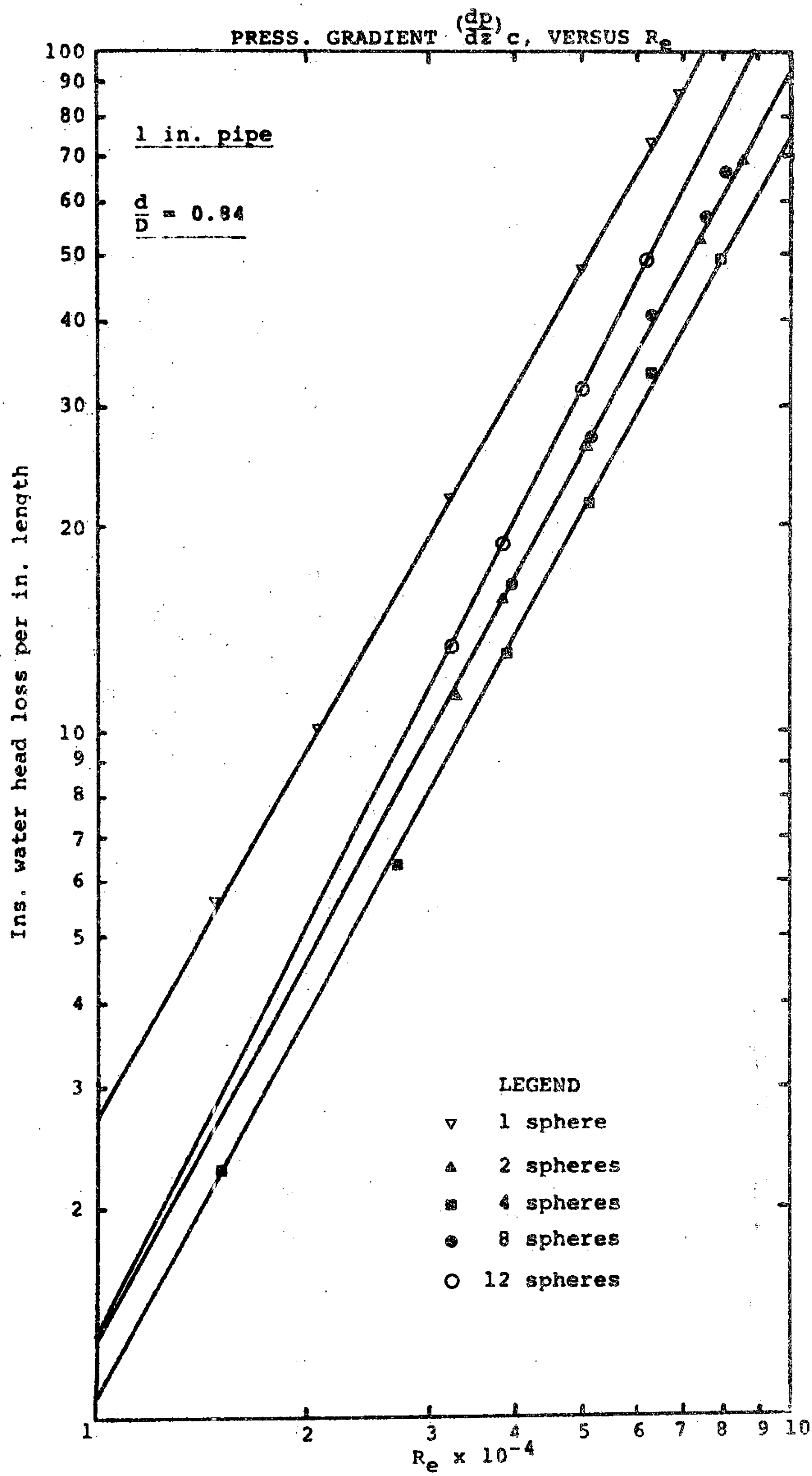
PRESS. GRADIENT $(\frac{dp}{dz})_c$, VERSUS R_e
1 in. pipe
$\frac{d}{D} = 0.84$
Ins. water head loss per in. length
$R_e \times 10^{-4}$
LEGEND
1 sphere
2 spheres
4 spheres
8 spheres
12 spheres

Fig. 12a.

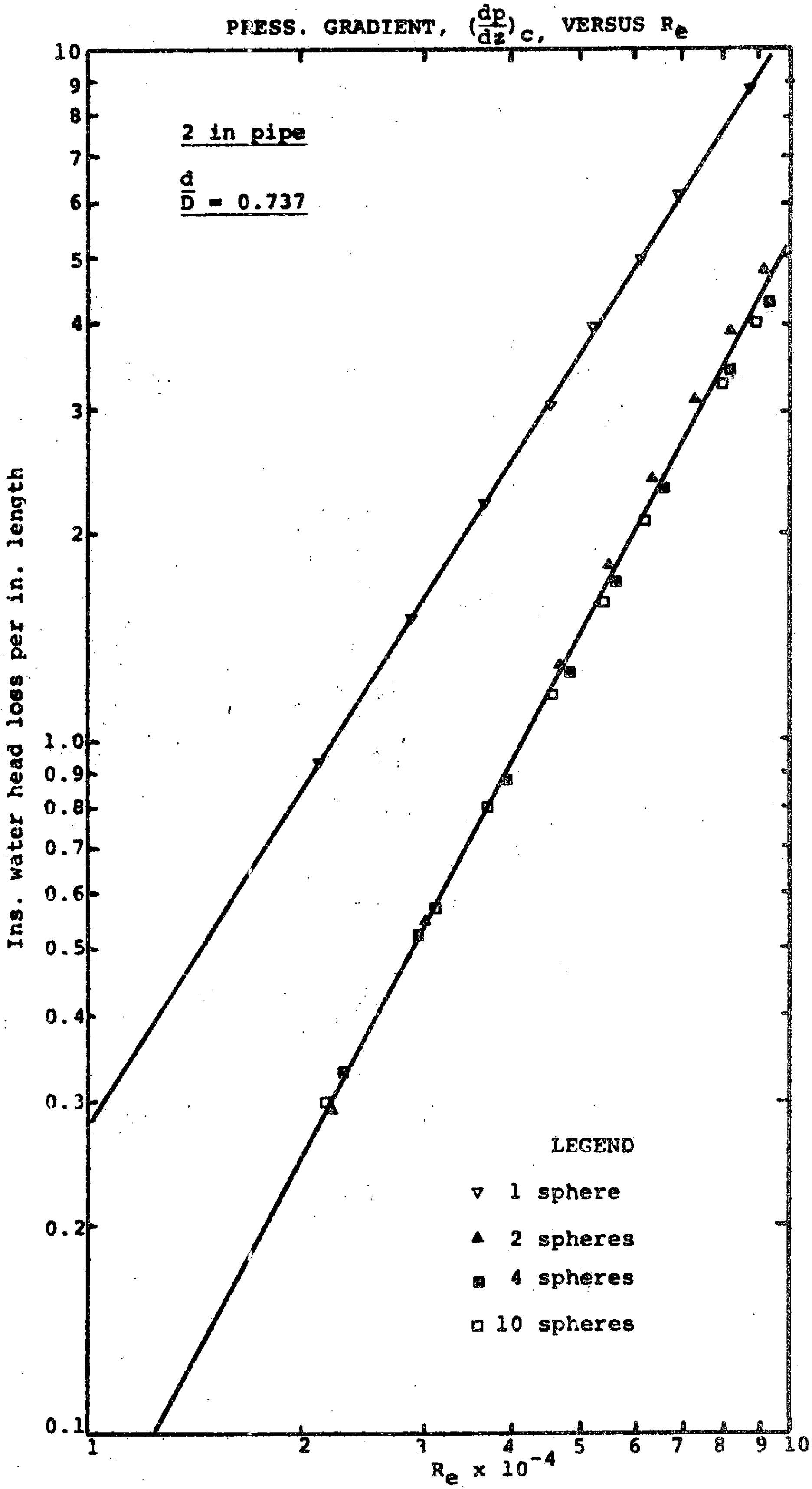
PRESS. GRADIENT, $(\frac{dp}{dz})_c$, VERSUS R_e
2 in pipe
$\frac{d}{D} = 0.737$
Ins. water head loss per in. length
$R_e \times 10^{-4}$
LEGEND
▽ 1 sphere
▲ 2 spheres
■ 4 spheres
□ 10 spheres

Fig. 12b.

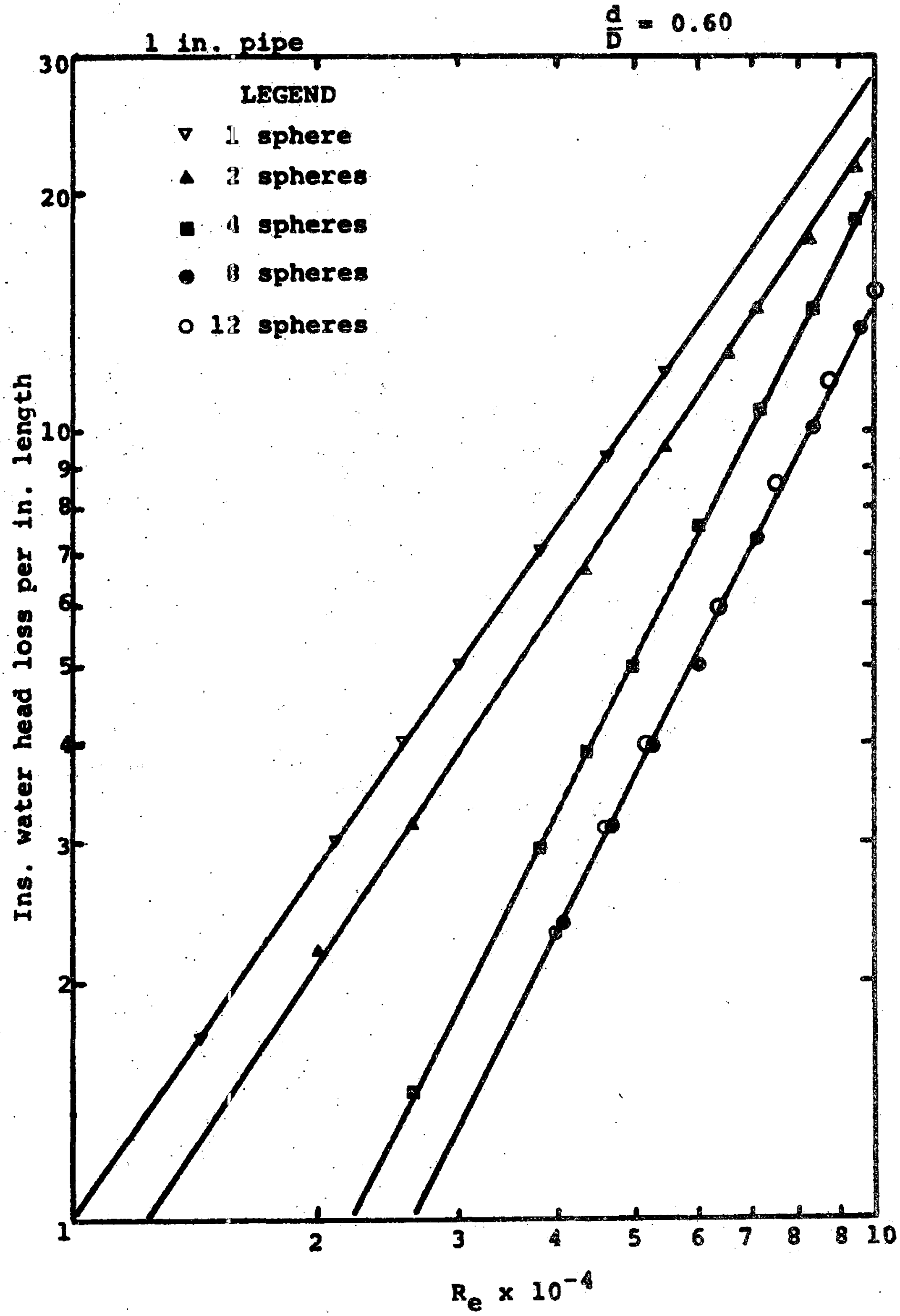

Fig. 12c. PRESS. GRADIENT, $(\frac{dp}{dz})_c$, VERSUS R_e

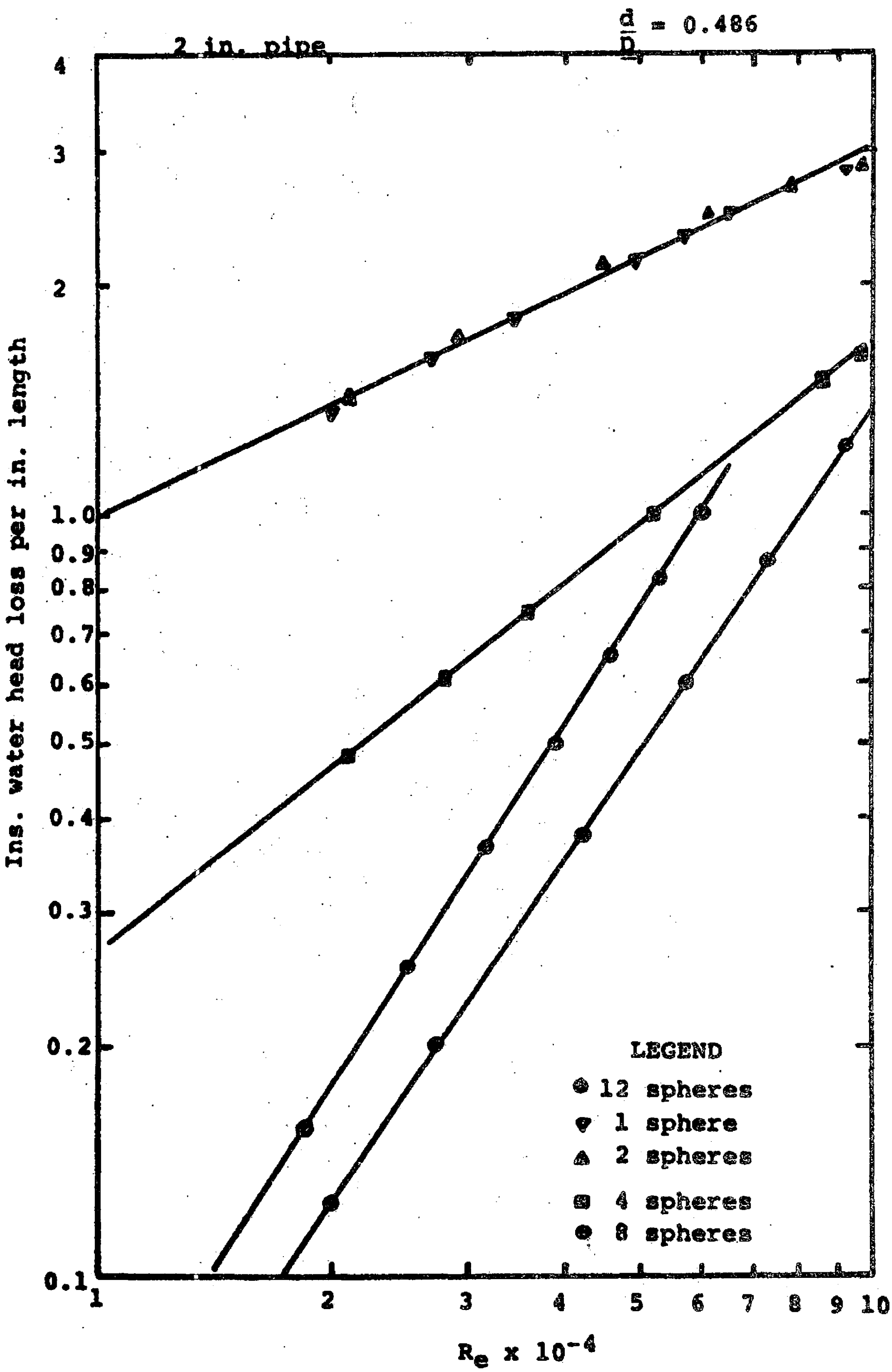

Fig. 12d. PRESS. GRADIENT, $(\frac{dp}{dz})_c$, VERSUS R_e

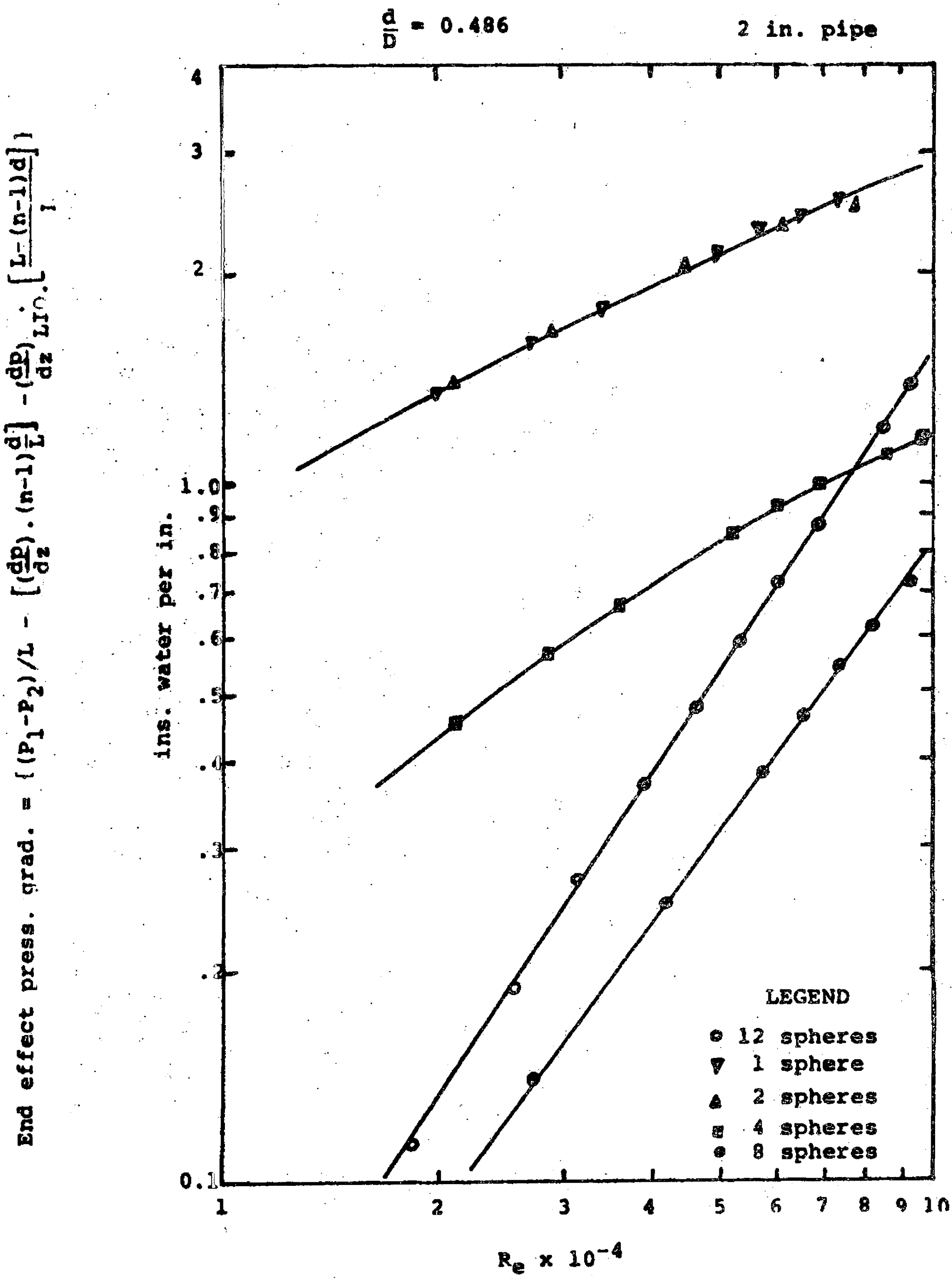

Fig. 13a END EFFECT PRESS. GRADIENT VERSUS R_e

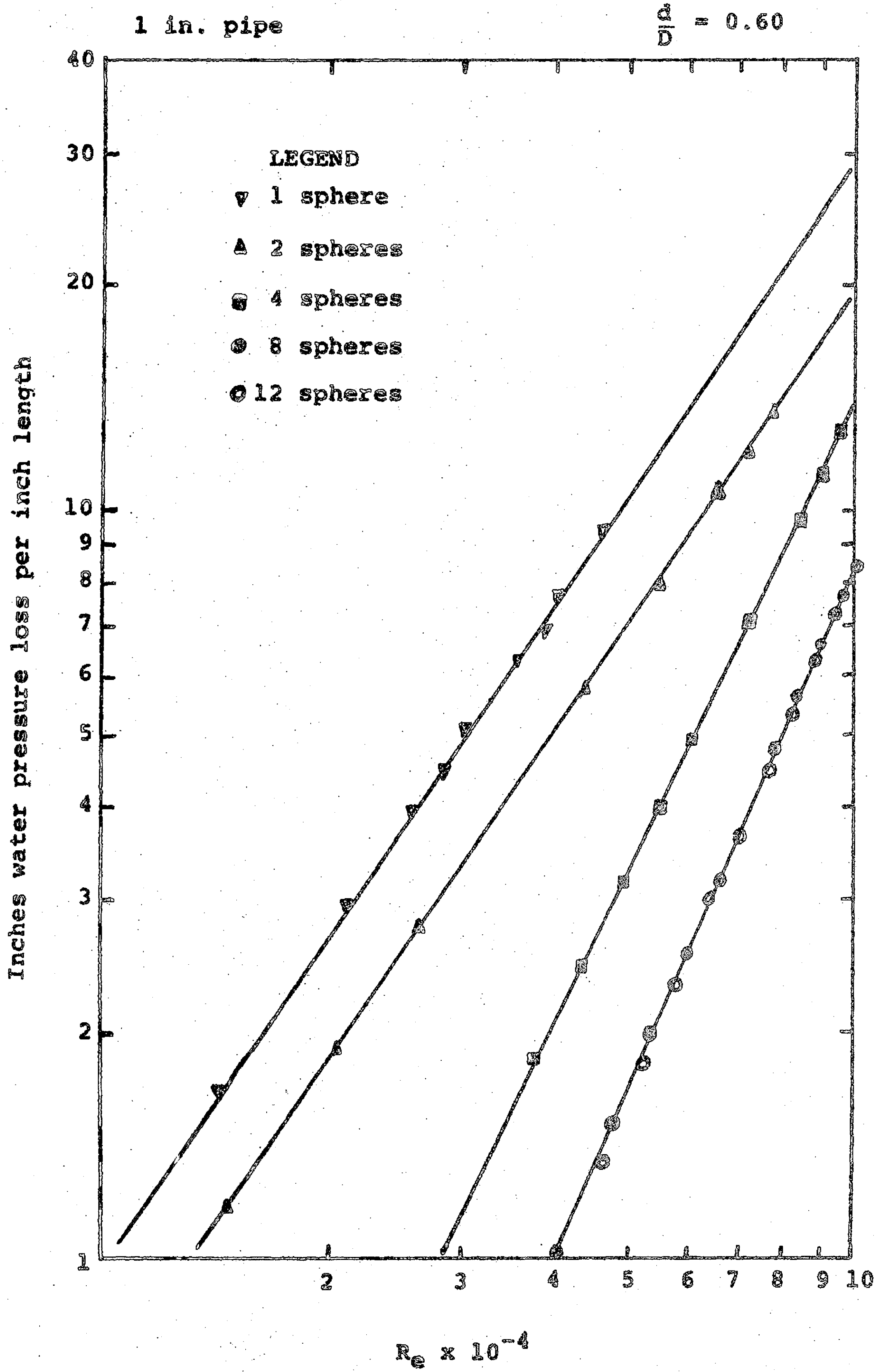

Fig. 13b END EFFECTS

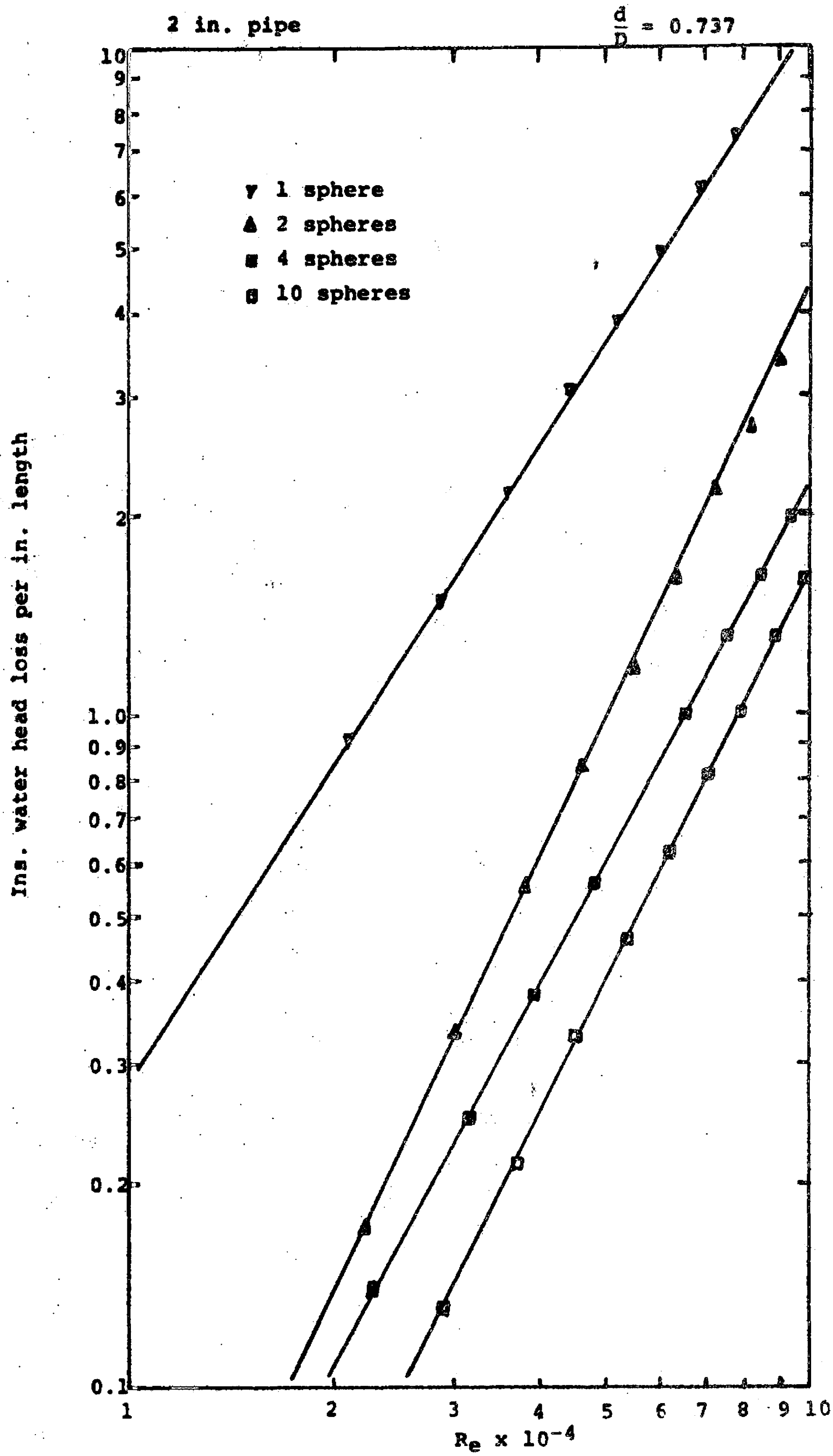

Fig. 13c. END EFFECTS

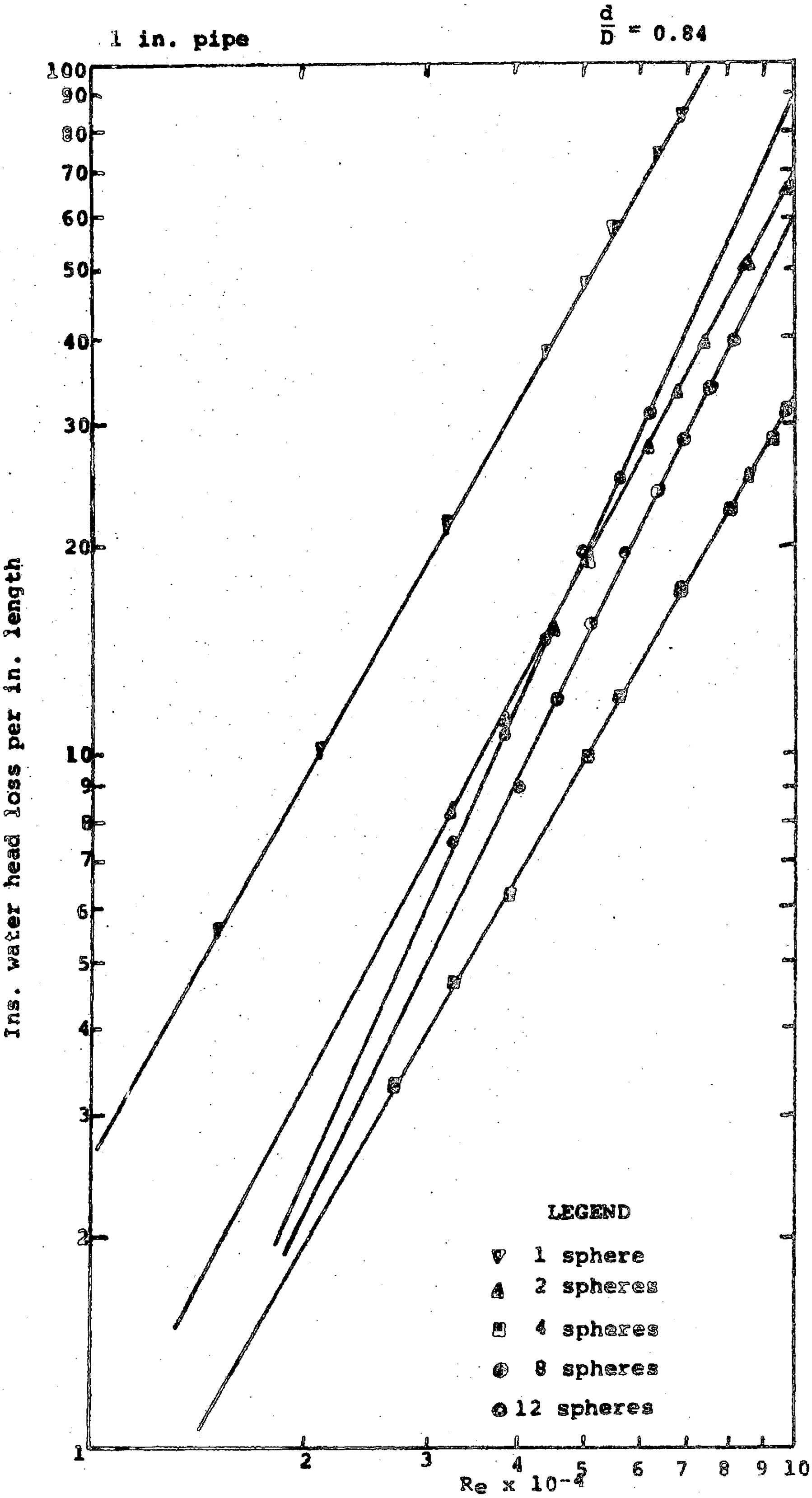

Fig. 13d. END EFFECT PRESSURE GRAD. VERSUS R_e

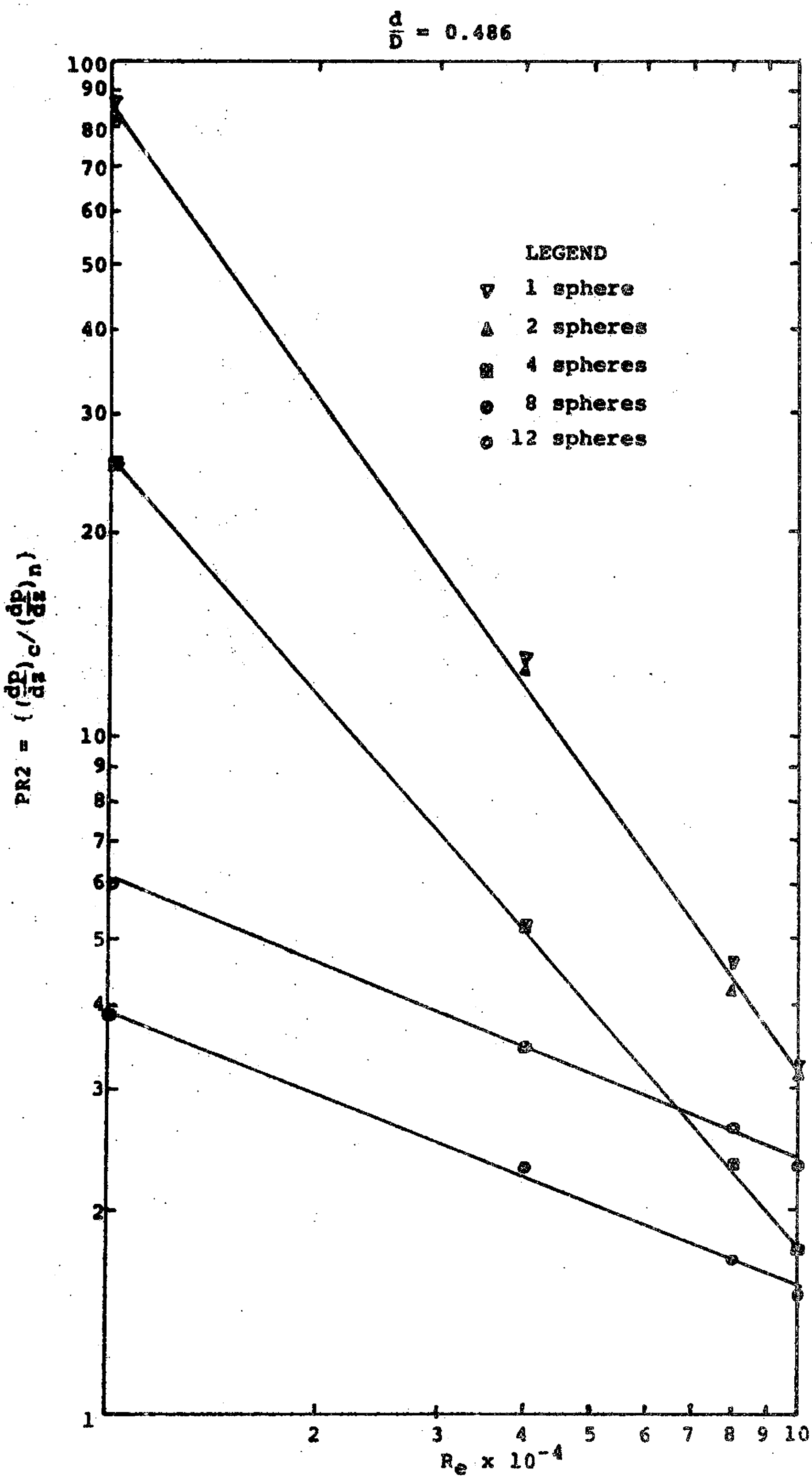

Fig. 14a PRESSURE RATIO, PR2, VERSUS R_e

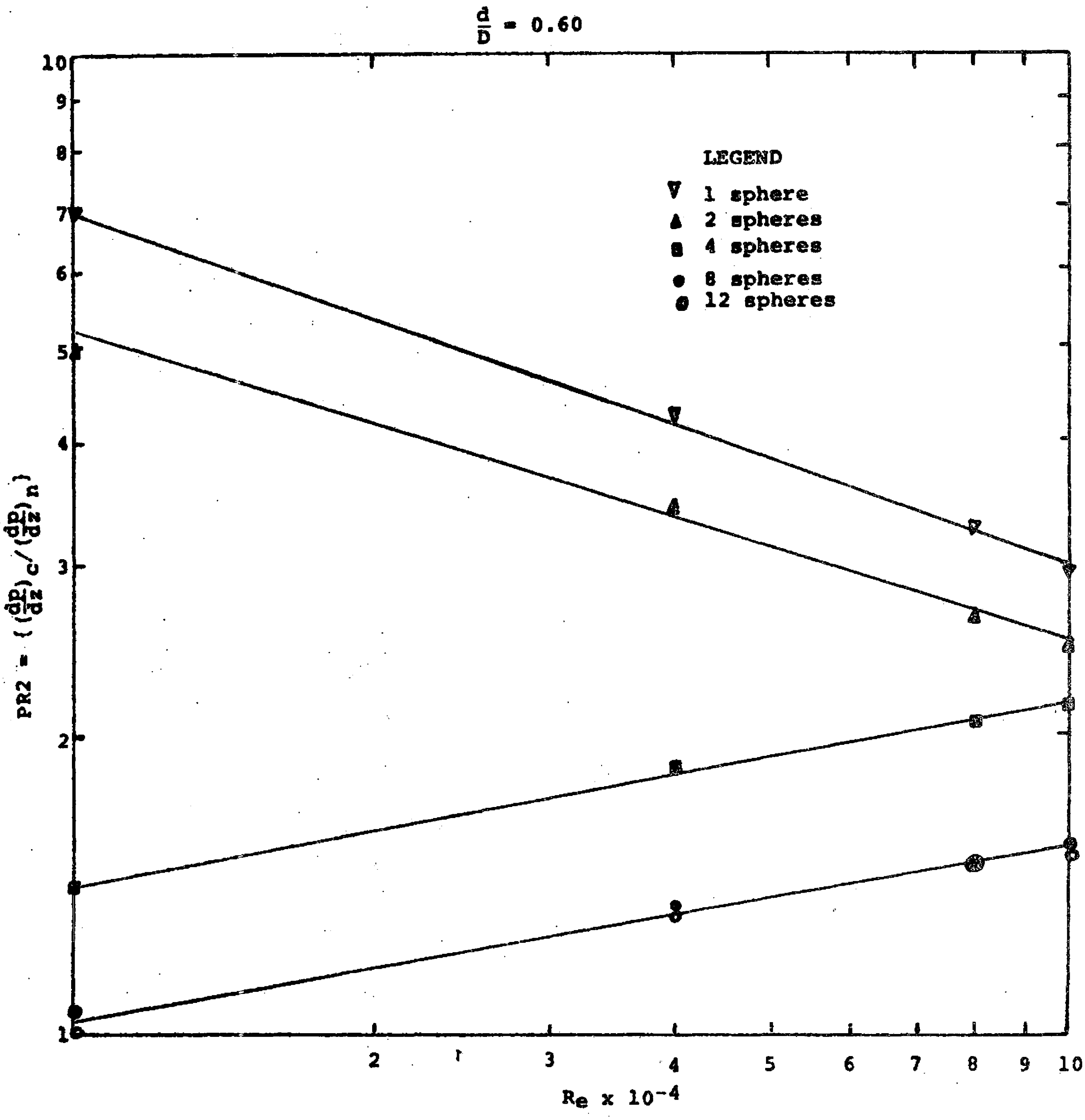

Fig. 14b PRESSURE RATIO, PR2, VERSUS R_e

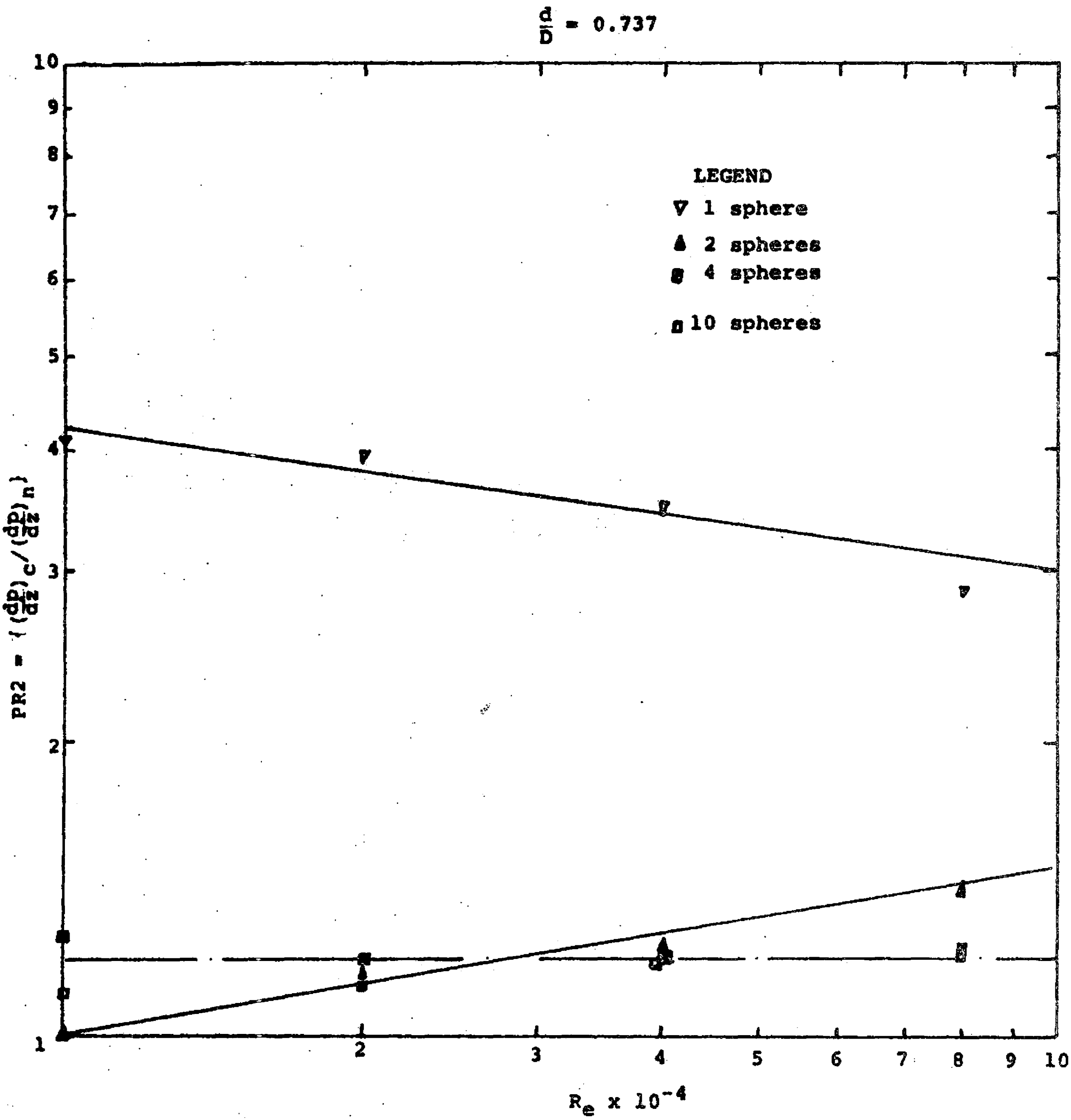

Fig. 14c PRESSURE RATIO, PR2, VERSUS R_e

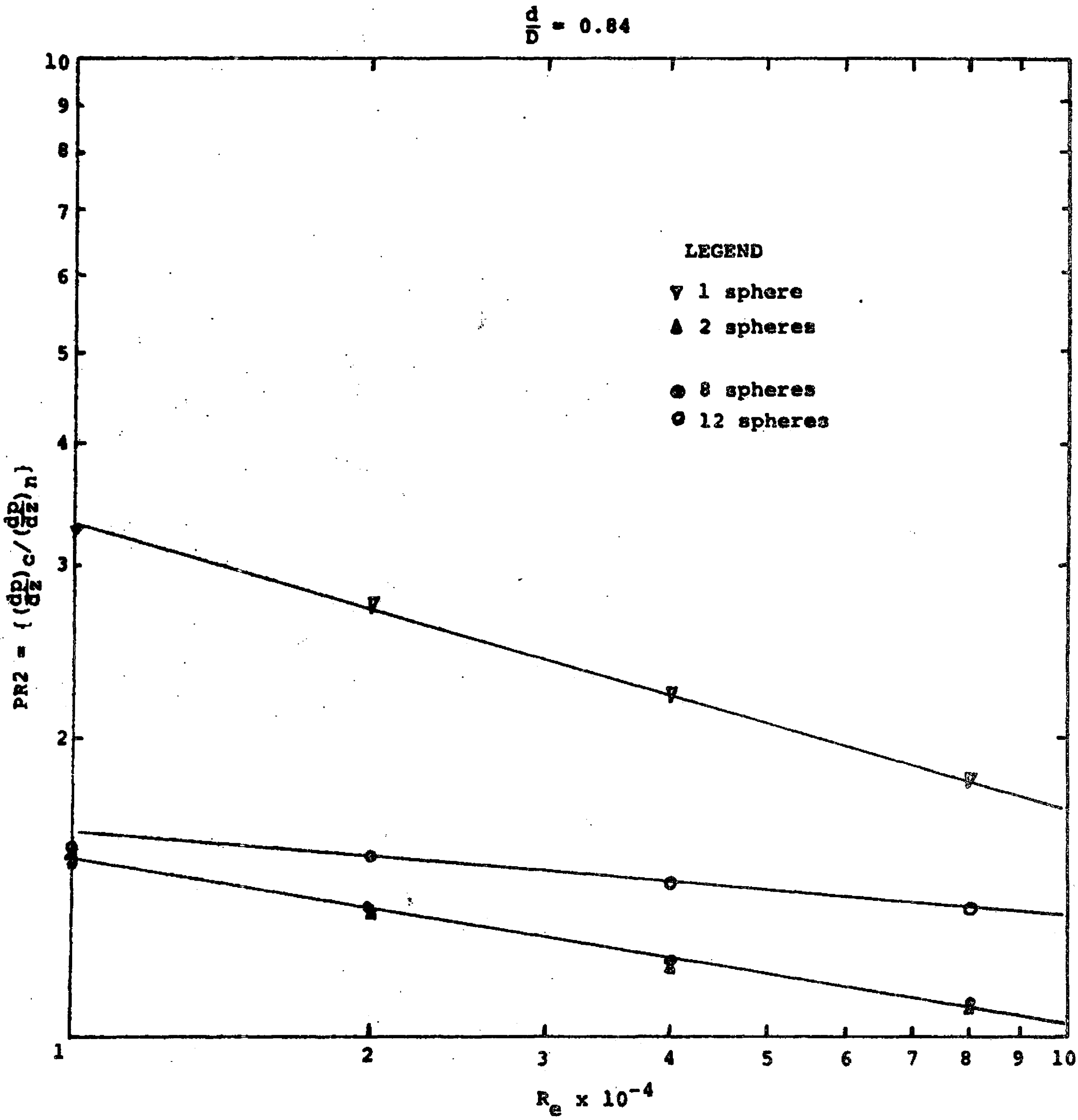

Fig. 14d PRESSURE RATIO, PR2, VERSUS R_e

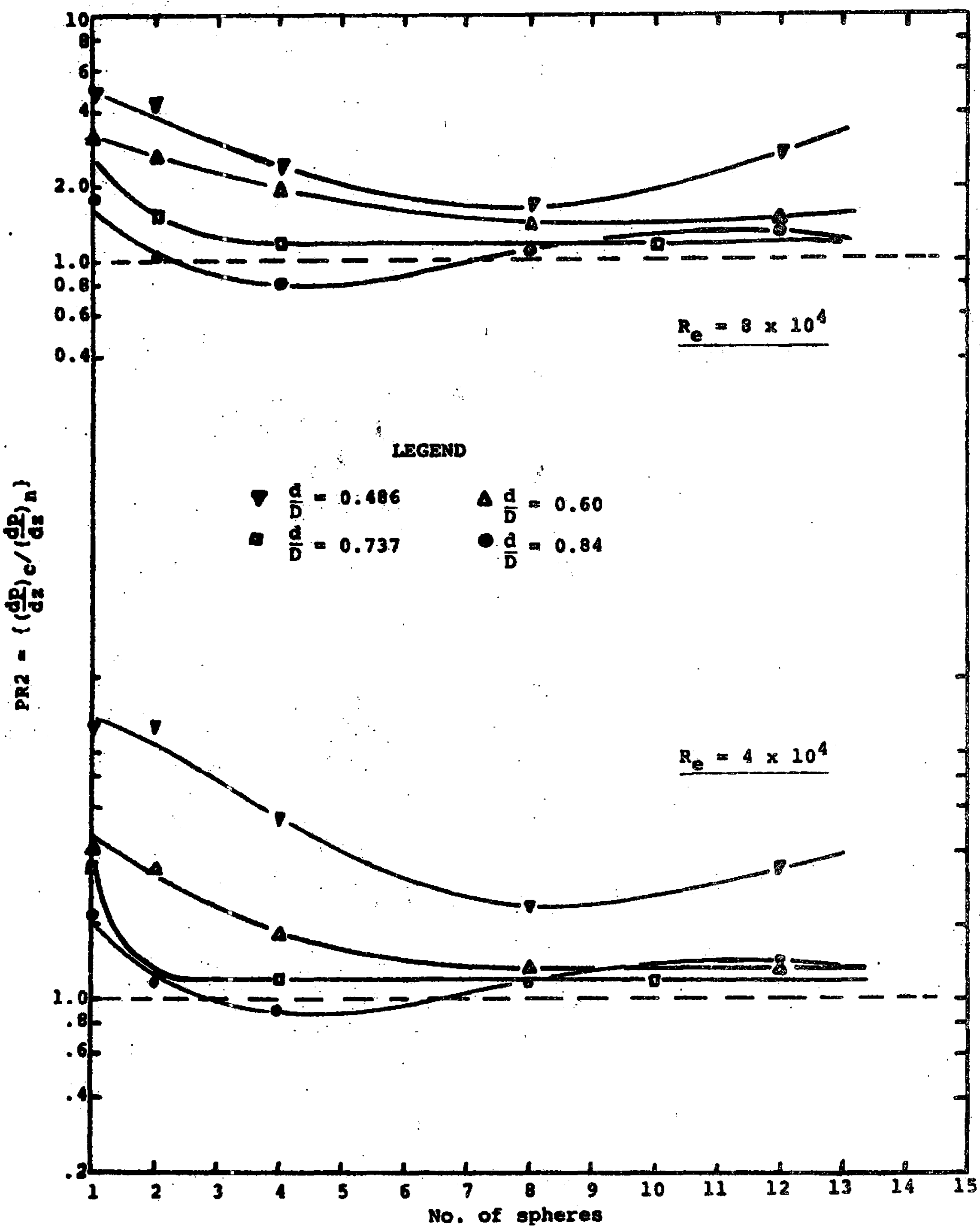

Fig. 15 PRESSURE RATIO, PR2, VERSUS No. OF SPHERES

Fig. 16a.

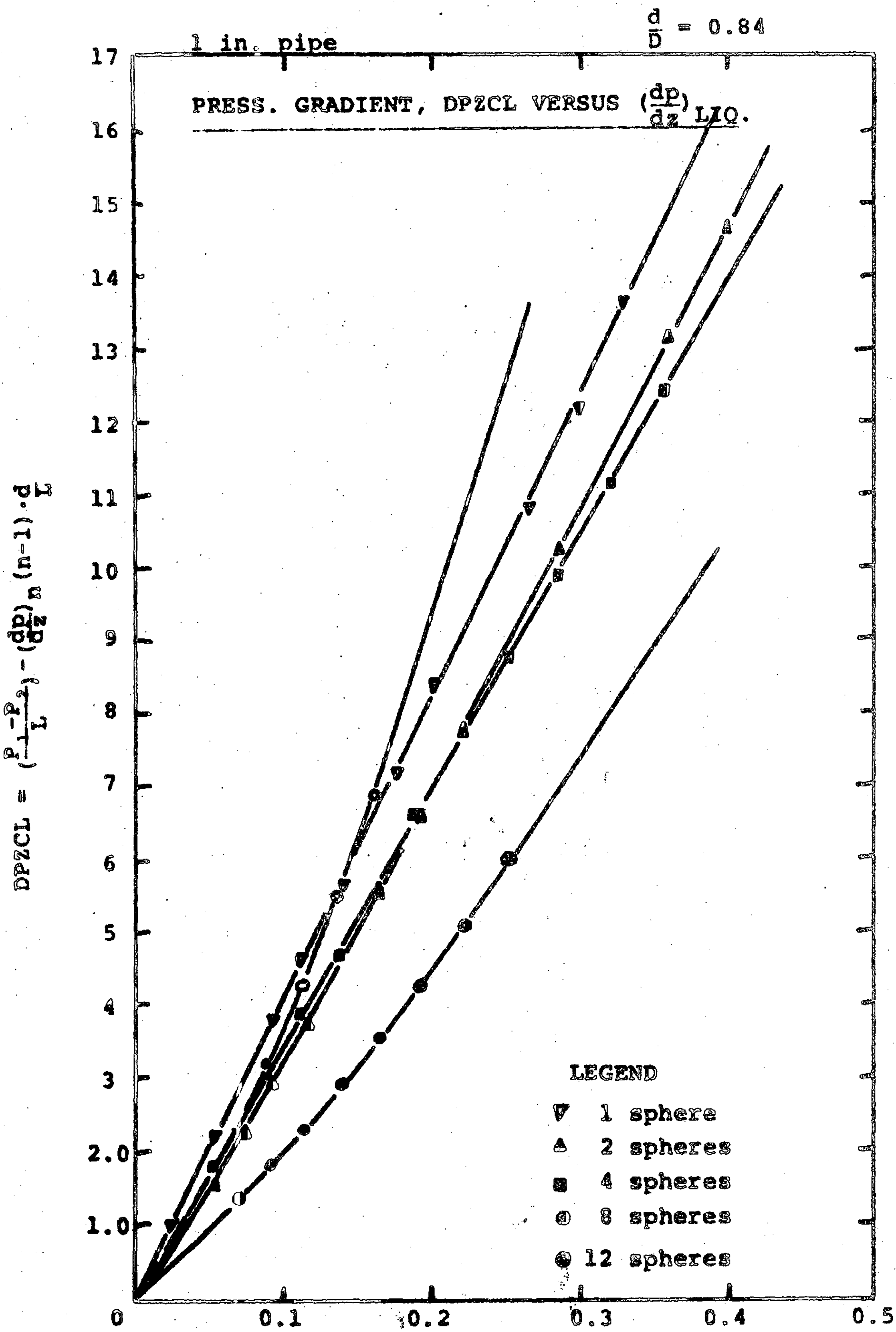

1 in. pipe
$\frac{d}{D} = 0.84$
PRESS. GRADIENT, DPZCL VERSUS $(\frac{dp}{dz})_{LIQ.}$
DPZCL = $(\frac{P_1 - P_2}{L}) - (\frac{dp}{dz})_n (n-1) \cdot \frac{d}{L}$
17
16
15
14
13
12
11
10
9
8
7
6
5
4
3
2.0
1.0
0
0.1
0.2
0.3
0.4
0.5
LEGEND
1 sphere
2 spheres
4 spheres
8 spheres
12 spheres

Fig. 16b.

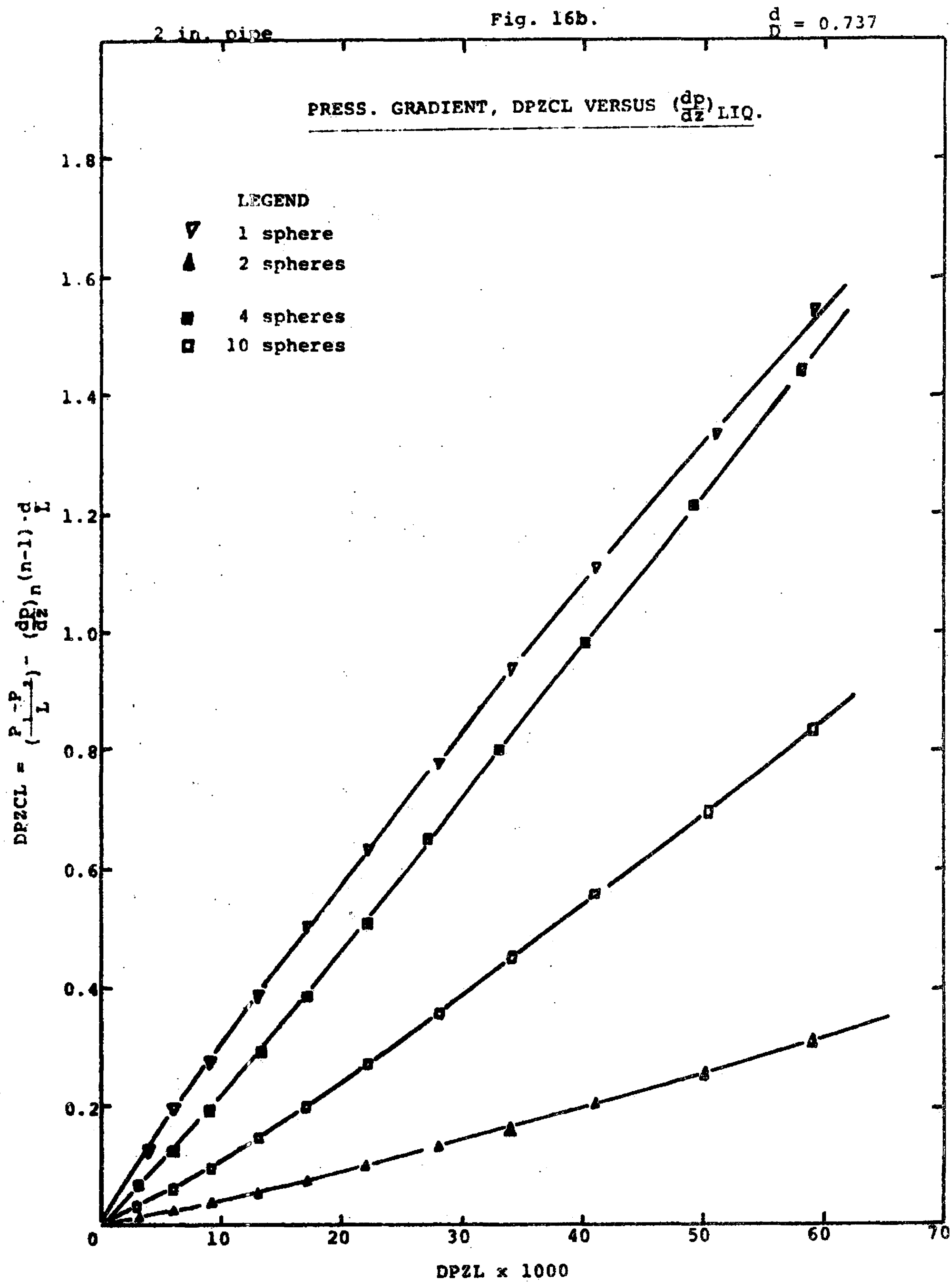
2 in. pipe
$\frac{d}{D} = 0.737$
PRESS. GRADIENT, DPZCL VERSUS $(\frac{dp}{dz})_{LIQ.}$
LEGEND
1 sphere
2 spheres
4 spheres
10 spheres
$DPZCL = (\frac{P_1 - P_2}{L}) - (\frac{dp}{dz})_n (n-1) \cdot \frac{d}{L}$
DPZL x 1000
0
10
20
30
40
50
60
70
0.2
0.4
0.6
0.8
1.0
1.2
1.4
1.6
1.8

Fig. 16c.

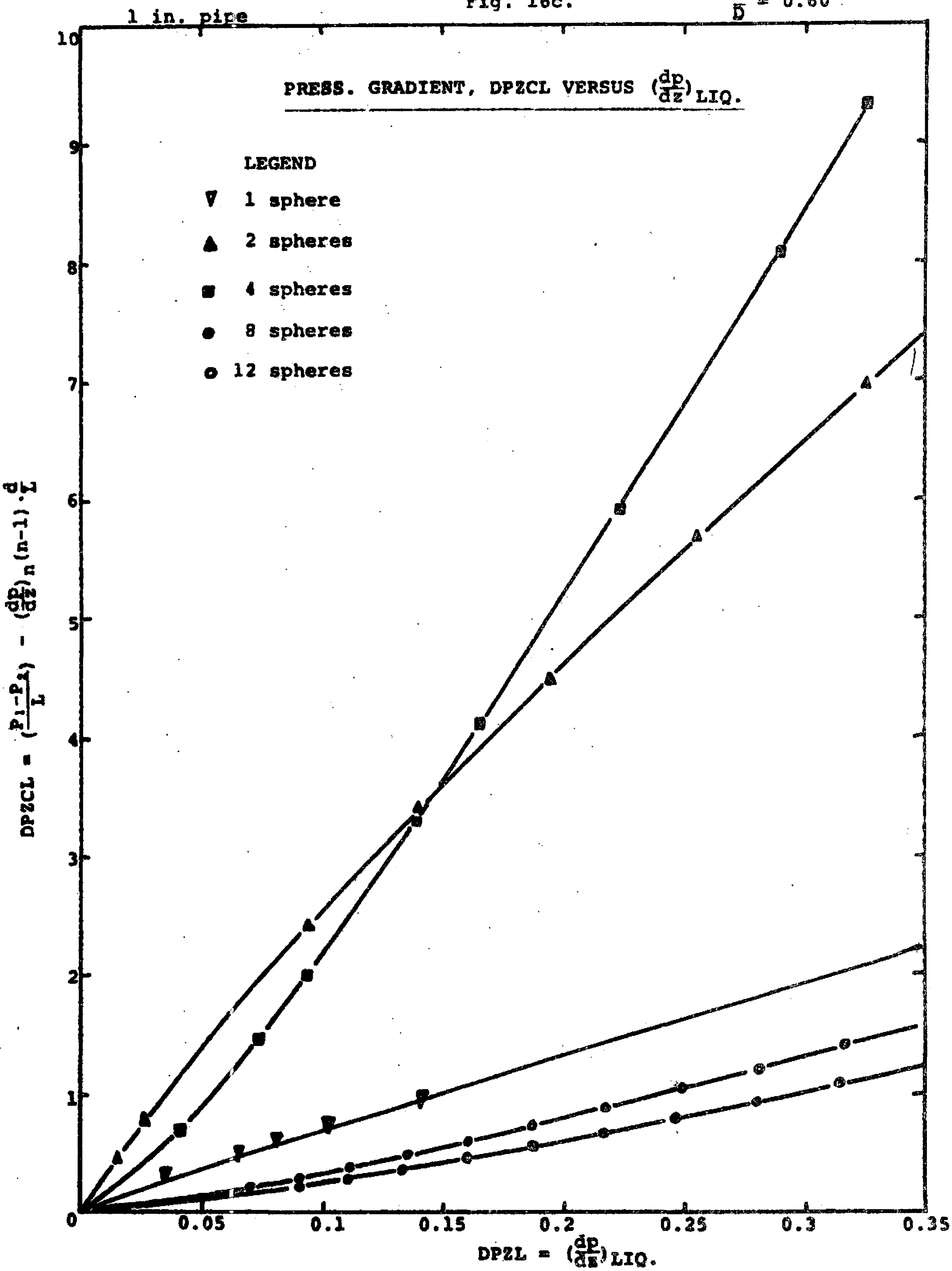

1 in. pipe
d/D = 0.60
PRESS. GRADIENT, DPZCL VERSUS $(\frac{dp}{dz})_{LIQ.}$
LEGEND
1 sphere
2 spheres
4 spheres
8 spheres
12 spheres
DPZCL = $(\frac{P_1-P_2}{L}) - (\frac{dp}{dz})_n (n-1)\cdot\frac{d}{L}$
DPZL = $(\frac{dp}{dz})_{LIQ.}$
0
0.05
0.1
0.15
0.2
0.25
0.3
0.35
1
2
3
4
5
6
7
8
9
10

Fig. 16d.

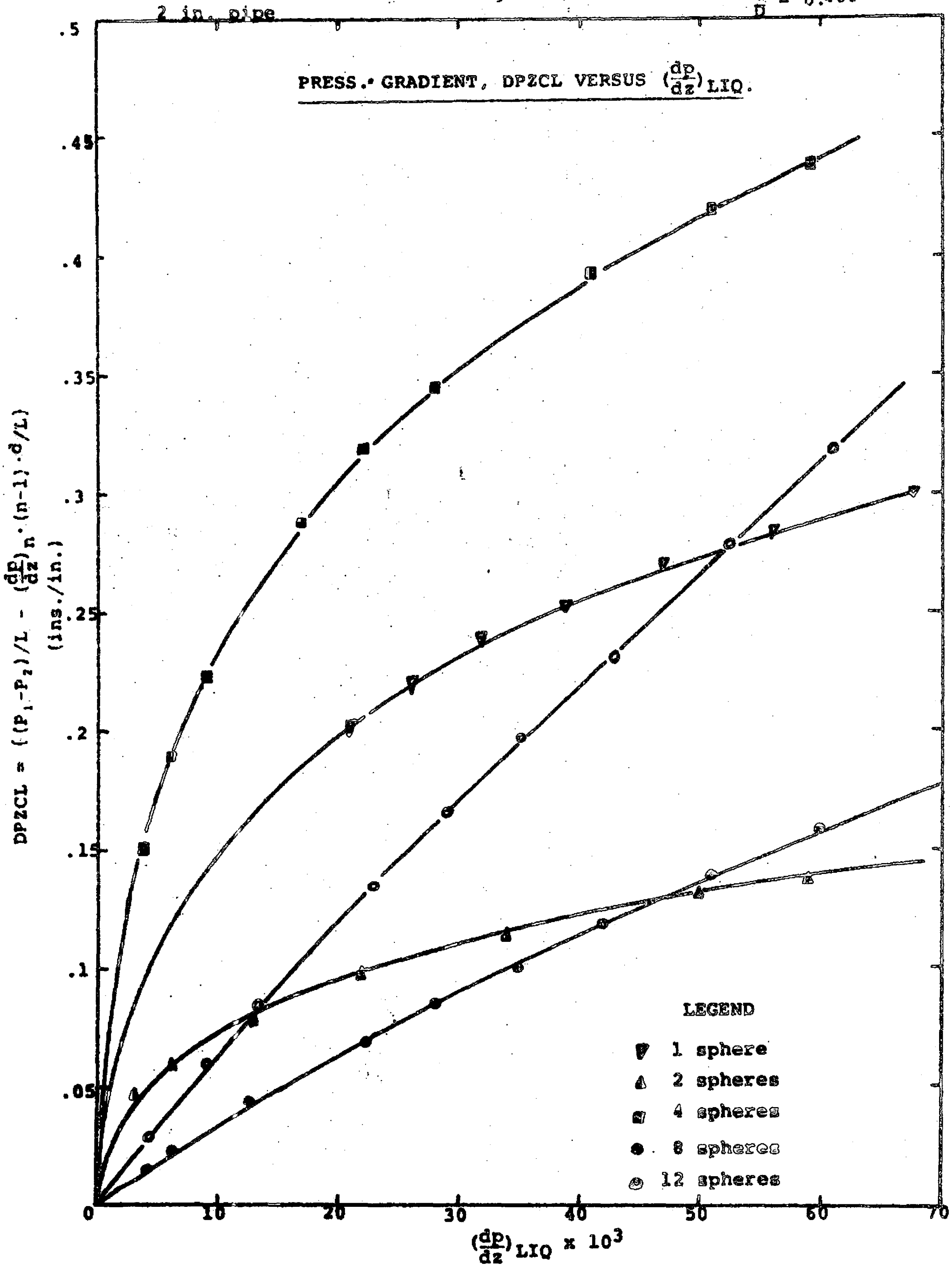
2 in. pipe
$\frac{d}{D} = 0.486$
PRESS. GRADIENT, DPZCL VERSUS $(\frac{dp}{dz})_{LIQ}$.
DPZCL = $((P_1-P_2)/L - (\frac{dp}{dz})_n \cdot (n-1) \cdot d/L)$ (ins./in.)
$(\frac{dp}{dz})_{LIQ} \times 10^3$
LEGEND
1 sphere
2 spheres
4 spheres
8 spheres
12 spheres
0
10
20
30
40
50
60
70
.05
.1
.15
.2
.25
.3
.35
.4
.45
.5

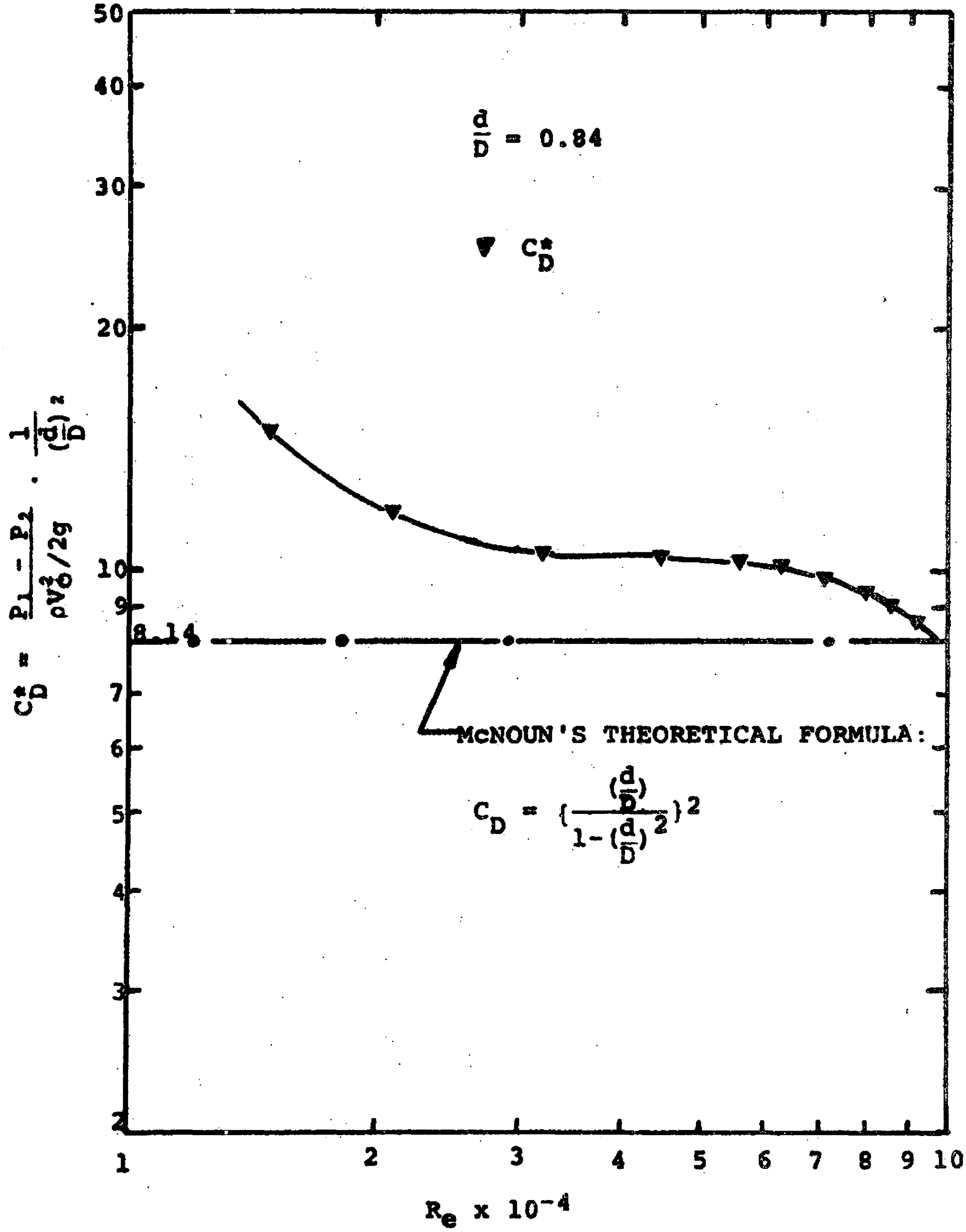

Fig. 17 DRAG COEFF., C_D^*, VERSUS R_e

5. DISCUSSION

5.1 Pressure Ratio, PR1, as a function of Reynolds Number and Diameter ratio

The experimental results for PR1 did not agree with equation (2.4.8), which expresses the pressure ratio, PR1, as a function of diameter ratio only. PR1 was observed to be a function of Reynolds number as well. The main explanation for this is that the theory assumes

$$\left.\begin{aligned} \left(\frac{P_{1n} - P_{2n}}{L}\right) &= F.\ R_{e_N}^{\ 1.75} \\ \text{and} \qquad \left(\frac{dp}{dz}\right)_{LIQ.} &= f.\ R_{e_N}^{\ 1.75} \end{aligned}\right] \qquad (5.1.1)$$

where F and f are functions of diameter ratio, kinematic viscosity and pipe diameter. In practice however, the exponent of R_{e_N} in equation (5.1.1.) is not necessarily 1.75. It varies between 1.5 and 2; as confirmed in reference No. 27.

Moreover, the equivalent diameter concept used in the analysis may not be applicable to annuli of this type, apart from the high Reynolds numbers involved. We, therefore, conclude that the theory has been over simplified and that the experimental values of PR1 are acceptable, within the limits of error estimated in section (4.4).

5.2. Pressure gradient DPZC and end effects, as a function of Reynolds number and number of spheres.

The graphs of DPZC and end effect versus Reynolds number, are very much what one would expect: the pressure gradient increases with increase of Reynolds number and diameter ratio, the plots are linear on a log-log scale and have varying intercepts and gradients, and the end effects diminish as the number of spheres in the train increases. Also the estimated error in the pressure gradient values obtained is relatively low - about 8%; signifying that figures 12 and 16 are quite reliable.

5.3 Pressure ratio, PR2, as a function of R_{e_N}, diameter ratio, and number of spheres.

Remembering that PR2 is the ratio of pressure gradient with end effects to the pressure gradient without end effects for a given sphere train, one would expect PR2 to tend to 1.0 as the number of spheres becomes very large. The lowest value of PR2 obtained for the maximum of 12 spheres was about 1.3. Taking into account the estimated error in PR2 of about 16%, the results suggest that we need more than 12 spheres for the lower limit in PR2 to be reached. That is, the end effects constitute still quite a significant part of the pressure gradient when the sphere train comprises 12 or less number of spheres.

5.4 Drag Coefficients

The discrepancy between the drag coefficients evaluated from data (with $\frac{d}{D} = 0.84$) and values corresponding to McNoun's formula lies well within the margin of error estimated in section (4.4.vii). Considering that the error in C_D could be as large as 33%, measuring pressure drops is obviously an inaccurate approach to finding the drag coefficients. In any case the formula,

$$C_D^* = \frac{D^2}{d^2} \cdot \frac{\text{Pressure Drop}}{Vo/2g}$$

can be applied only for single spheres and diameter ratios greater or equal to 0.8. It seems therefore, that the best method of obtaining drag coefficients for sphere trains like this is to measure the drag directly using a force transducer. We suggest that the test sections be redesigned so that measurements of force on the sphere trains can be made.

5.5 Optimum Diameter Ratio for Sphere Trains

The horsepower / unit mass flow rate is an important parameter relating to the economy of a capsule or solids pipeline. A minimum value of the parameter is usually desired.

The results presented in section 4.6 indicate that for spherical capsules the optimum diameter ratio (sphere / pipe) is 0.5 for the above parameter to be minimum. In practice, however, we would recommend a diameter ratio of about 0.6 as this would reduce the tendency for the spheres to ride one above the other.

6. CONCLUSIONS

On the basis of the analyses and experimental results presented above, the following conclusions can be made:

(i) The hydraulic gradient in smooth pipes containing sphere trains is a logarithmic function of the Reynolds number as shown in Figs. 12(a-d) for 1" and 2" pipes, and Reynolds numbers between 10^4 and 10^5. It tends to increase with increase in diameter ratio, and decrease with increase in the number of spheres, for any given pipe diameter and Reynolds number.

(ii) For long sphere trains, the ratio of the pressure gradient with spheres located in the pipe to the free-pipe pressure gradient can be approximated by the regression equation:-

$$PR1 = 259.13\left(\frac{d}{D}\right)^{4.543}\left(Re_{N} \cdot 10^{-4}\right)^{c}$$

where c varies between 0 and 0.33 given that $0.84 \geqslant \left(\frac{d}{D}\right) \geqslant 0.486$ and $10^4 \leqslant R_{e_N} \leqslant 10^5$.

(iii) End effects diminish from 100% of the total pressure gradient to about 20% as the number of spheres comprising the sphere train increases from 1 to 12.

(iv) The drag coefficients estimated from pressure drop measurements for 1 sphere compare well with McNoun's drag coefficients only for the highest sphere-to-pipe diameter ratio used, 0.84. For diameter ratios less than 0.8, drag coefficients cannot be accurately evaluated from pressure drops.

(v) By using the results presented in Figs. 10, 11 and 14, the pressure drop due to a sphere train located in a pipe of any diameter can be estimated as illustrated in section 4.5; given that the sphere-to-pipe diameter ratio lies between 0.486 and 0.84, for the Reynolds number range $10^4 - 10^5$.

REFERENCES

(1) BRENNER, H, "Slow Viscous Flow past a Sphere in a Cylindrical Tube", Journal of Fluid Mechanics, Volume 4, 1958, pages 195-213

(2) FOXEN, H, "The Motion of a Rigid Sphere along the Axis of a Pipe filled with Viscous Fluid", Arkiv. Math. Astron. Fysik. Volume 17(27),1923, pages 1-28. (In German.)

(3) FAYON, A.M. and HAPPEL, John, "Effect of a Cylindrical Boundary on a Fixed Rigid Sphere in a Moving Viscous Fluid", American Institute of Chemical Engineers, Journal, Volume 6(1), 1960, pages 55-58.

(4) HAPPEL, John and BYRNE, B.J., "Motion of a Sphere and Fluid in a Cylindrical Tube", Industrial and Engineering Chemistry, Volume 46(6), 1954, pages 1181-1186.

(5) PLISKIN, Irwin, and BRENNER, Howard, "Experiments in the Pressure Drop created by a Sphere settling in a Viscous Liquid", Journal of Fluid Mechanics, Volume 7(1), 1963, pages 89-96.

(6) TANEDA, S., "Experimental Investigations of the wake behind a Sphere at low Reynolds Numbers", Journal of the Physical Society of Japan, Volume 11(10), 1956, pages 1104-1108.

(7) WAGENER, P.P. and ASHKERAS, Harry, "Wind Tunnel Measurements of Sphere Drag at Supersonic Speeds amd low Reynolds numbers", Journal of Fluid Mechanics, Volume 10(4),1961, pages 550-560.

(8) SRIMATHI, C.R. and BHAT, G.N., "Drag Interaction Effects in Linear Sphere Assemblies", British Journal of Applied Physics, Volume 16, 1965, pages 551-556.

(9) ERICHHORN, R. and SMALL, S., "Experiments in the Lift and Drag of Spheres Suspended in a Poiseuille Flow", Journal of Fluid Mechanics, Volume 20(3), 1964, pages 513-522.

(10) ERESON, G.F., "Interaction between two equal-sized equal-settling Spheres moving through a Viscous Liquid", British Journal of Applied Physics, Volume 11, 1960, pages 87-88.

(11) ERESON, G.F., HALL, E.N., and WARD, S.G., "Interaction between two equal sized settling Spheres moving through a Viscous Liquid", British Journal of Applied Physics, Volume 10(1), 1959, pages 43-47.

(12) FIDLERIS, V.and WHITMORE, R.L.,"Experimental Determination of the Wall Effect for Spheres falling anially in Cylindrical Vessels", British Journal of Applied Physics, Volume 12(9), 1961, pages 490-494.

(13) HAPPEL, John, and PFEFFER, Robert, "The Motion of two Spheres following each other in a Viscous Fluid", American Institute of Chemical Engineers, Journal, Volume 6(1), 1960, pages 129-133.

(14) McNOUN, J.S.,LEE. H.M., McPHERSON. M.B. and ENGEZ, S.M., "Influence of Boundary Proximity on the Drag of Spheres", Proc. 7th. Interim Congress of Applied Mechanics.(London), 2, 1948, pages 17-29.

(15) McNOUN, J.S. and NEWLIN, J.T. "Drag on Spheres within Cylindrical Boundaries", Proc. 1st. U.S. National Congress of Applied Mechanics,(Chicago, Ill.) 1951, pages 801-806.

(16) HODGSON, G.W. and CHARLES, M.E., "The Pipeline Flow of Capsules; Part 1: The Concept of Capsule Pipelining", Canadian Journal of Chemical Engineering, Volume 41, 1963, pages 43-45.

(17) CHARLES, M.E., "The Pipeline Flow of Capsules; Part 2: Theoretical Analysis of the Concentric Flow of Cylindrical Forms", Canadian Journal of Chemical Engineering, Volume 41(2), 1963, pages 46-51.

(18) ELLIS, H.S., "The Pipeline Flow of Capsules; Part 3: An Experimental Investigation of the Transport by Water of Single Cylindrical and Spherical Capsules with Density

equal to that of the Water", Canadian Journal of Chemical Engineering, Volume 42(1), 1964, pages 1-8.

(19) ELLIS, H.S., "The Pipeline Flow of Capsules; Part 4: An Experimental Investigation of the Transport in Water of Single Cylindrical Capsules with Density greater than that of Water", Canadian Journal of Chemical Engineering, Volume 42(2), 1964, pages 69-76.

(20) ELLIS, H.S., "The Pipeline Flow of Capsules; Part 5: An Experimental Investigation of the Transport by Water of Single Spherical Capsules with Density greater than that of the Water", Canadian Journal of Chemical Engineering, Volume 42(4), 1964, pages 155-161.

(21) NEWTON, R., REDBERGER, P.J. AND ROUND, G.F., "The Pipeline Flow of Capsules; Part 6: Numerical Analysis of some Variables determining Free Flow", Canadian Journal of Chemical Engineering, Volume 42(4), 1964, pages 168-173.

(22) ELLIS, H.S. and BOLT, L.H., "The Pipeline Flow of Capsules; Part 7: An Experimental Investigation of the Transport by two Oils of Single Cylindrical and Spherical Capsules with Density equal to that of the Oil", Canadian Journal of Chemical Engineering, Volume 42(5), 1964, pages 201-210.

(23) ROUND, G.F. and BOLT,L.H., "The Pipeline Flow of Capsules; Part 8: An Experimental Investigation of the Transport

in Oil of Single, Denser-than-Oil Spherical and Cylindrical Capsules", Canadian Journal of Chemical Engineering, Volume 43(4), 1965, pages 197-205.

(24) JAN KRUYER, REDBERGER, P.J. and ELLIS, H.S., "The Pipeline Flow of Capsules; Part 9", Journal of Fluid Mechanics, Volume 30(3), 1967, pages 513-531.

(25) HINZE. J.O., "Turbulence", McGraw-Hill Book Co., 1959, pages 517-518.

(26) KNUDSEN, J.G. and KATZ, D.L., "Fluid Dynamics and Heat Transfer", Chemical Engineering Series, McGraw-Hill Book Co., 1958, pages 158-164.

(27) STREETER, "Fluid Mechanics", McGraw-Hill, 3rd, Edition, pages 184-186, and 188.

(28) ROUND, G.F. and KRUYER, J. "Experiments on the Suspension of Spheres in Inclined Tubes - Suspension by Water in Turbulent Flow", Chemical Engineering Science, Volume 22, 1967, pages 1133-1145.

APPENDICES

A. 1 CALCULATION OF THE REYNOLDS NUMBER FROM FLOW RATE, PIPE DIAMETER, AND TEMPERATURE MEASUREMENTS.

Mean velocity, $V_o = \frac{4Q'}{\pi D^2} \times 144$ ft/sec where Q is in ft^3/sec. and D is in inches.

1 cu. ft/sec. = 373.733 Imperial gall./min.

$$V_o = \frac{4 \times 144\ Q}{\pi \times 373.73\ D^2} \text{ ft/sec. where Q is in Imperial gall./min.}$$

$$V_o = \frac{0.4905\ Q}{D^2} \text{ ft/sec.}$$

$$R_e = \frac{V_o\ D'}{\nu}$$

where ν (ft^2/sec.) is the kinematic viscosity at the temperature, T, measured, and D' is in ft.

$$= \frac{V_o\ D}{12\nu}$$

Substituting for V_o,

$$R_e = 0.04083\left(\frac{Q}{\nu . D}\right)$$

A.2 Derivation of Equation (5.5.1)

$$\text{Horsepower / ft.} = \beta_1 (PR1) \left(\frac{dp}{dz} \right)_{LIQ} \times \text{Flow rate}$$

where β_1 is a constant.

$$\text{Flow rate} = V_o \cdot \frac{\pi D^2}{4} = \left(R_e \cdot \frac{\nu}{D}\right) \cdot \frac{\pi D^2}{4} = \frac{\pi D \nu}{4} \cdot R_e$$

$$\therefore \text{ Horsepower / ft} = \beta_1 \cdot (PR1) \left(\frac{dp}{dz}\right)_{LIQ} \cdot \frac{\pi \nu D}{4} \cdot R_e$$

$$\text{Mass flow rate} = \frac{\text{Capsule mass}}{d} \times V_c = \frac{\frac{4}{3}\pi\left(\frac{d}{2}\right)^3 \cdot V_c}{d}$$

where V_c is the capsule velocity.

$$\therefore \frac{\text{H.P./ft}}{\text{(tons/sec.)}} = \frac{\beta_2 \cdot (PR1) \left(\frac{dp}{dz}\right)_{LIQ} \cdot D \cdot R_e}{d^2 \cdot V_c}$$

where β_2 is a constant.

At any specified Reynolds number, we can take $\left(\frac{dp}{dz}\right)_{LIQ}$ as constant. So also is the capsule velocity, V_c.

$$\frac{\text{H.P./ft}}{\text{(tons/sec.)}} = \beta_3 \cdot (PR1) \cdot \frac{D}{d^2} = \beta_3 \cdot \frac{PR1}{D\left(\frac{d}{D}\right)^2}$$

Given any pipe diameter, therefore,

$$\frac{\text{H.P./ft.}}{\text{(tons/sec.)}} = \beta \cdot \frac{PR1}{(d/D)^2}$$

where β is a constant.